

12-2012

# DETERMINATION OF A HIGHER-ORDER ELASTIC CONSTANT OF A SINGLE FILAMENT OF HEXTOW IM7-12K CARBON FIBER USING FINITE DEFORMATIONS

Luciana Oliveira  
Clemson University, cordeoli@gmail.com

Follow this and additional works at: [https://tigerprints.clemson.edu/all\\_theses](https://tigerprints.clemson.edu/all_theses)

 Part of the [Materials Science and Engineering Commons](#)

---

## Recommended Citation

Oliveira, Luciana, "DETERMINATION OF A HIGHER-ORDER ELASTIC CONSTANT OF A SINGLE FILAMENT OF HEXTOW IM7-12K CARBON FIBER USING FINITE DEFORMATIONS" (2012). *All Theses*. 1525.  
[https://tigerprints.clemson.edu/all\\_theses/1525](https://tigerprints.clemson.edu/all_theses/1525)

This Thesis is brought to you for free and open access by the Theses at TigerPrints. It has been accepted for inclusion in All Theses by an authorized administrator of TigerPrints. For more information, please contact [kokeefe@clemson.edu](mailto:kokeefe@clemson.edu).

DETERMINATION OF A HIGHER-ORDER ELASTIC CONSTANT OF A SINGLE  
FILAMENT OF HEXTOW<sup>®</sup> IM7-12K CARBON FIBER USING FINITE  
DEFORMATIONS

---

A Thesis  
Presented to  
the Graduate School of  
Clemson University

---

In Partial Fulfillment  
of the Requirements for the Degree  
Master of Science  
Materials Science and Engineering

---

by  
Luciana Correa de Oliveira  
December 2012

---

Accepted by:  
Dr. Apparao Rao, Committee Chair  
Dr. Malcolm Skove  
Dr. Konstantin Kornev  
Dr. Igor Luzinov  
Dr. Jian Luo

## ABSTRACT

The modulus of elasticity of a homogeneous body is the same for all directions. No known crystalline materials have a Young's modulus that is the same in all directions. The linear theory of elasticity states that strain is proportional to stress so that a straight line is obtained in a stress *versus* strain plot. As long as the forces applied to the body are proportional, the body behaves perfectly elastically, obeying Hooke's law. At high enough strains, however, deviations from Hooke's law will occur. Nonlinear elasticity is generally apparent when large deformations are applied and usually when the sample size is on the micro/nano scale. The nonlinear theory of elasticity of materials is more complex and leads to the introduction of higher-order elastic constants. These higher-order constants confer increased accuracy to theoretical predictions of the elastic behavior of the material. Here, equipment specifically designed for the tensile measurements of individual micro/nano-composite fibers will be introduced. The results obtained for the elastic properties of single filaments of IM7 carbon fibers, which include the usual second-order as well as the third-order elastic constants and the piezoresistivity will be presented.

## ACKNOWLEDGMENTS

I would like to immensely thank my advisor, Professor A. Rao for his support and encouragement during the course of my research. My deepest gratitude is also extended to Professor M. Skove who guided me throughout the development of this project and who has provided rich discussions. I am very thankful for the dedicated time, lessons of life and the opportunity given by both of you of making me part of this incredible research group.

I would like to acknowledge Professors K. Kornev, I. Luzinov and J. Luo for all your help and advice serving on my research committee.

I would like to thank all sources of financial support that were essential during my stay at Clemson. Thanks to the Department of Materials Science and Engineering for the teaching assistantship during my first year and, many thanks to Dr. L. Dooley from the Dean's Office for Research and Graduate Studies, Dr. Anvar Zakhidov from University of Texas at Dallas and, Dr. Steven Serkiz from Savannah River National Laboratory for my research assistantship.

My heartfelt thanks are offered to everyone who directly or indirectly has contributed to my research projects and academic achievements: Dr. R. Podila, Dr. J. Reppert, Dr. K. Yang, Dr. J. Gaillard, D. Saini, H. Behlow, K. Lingam, M. Karakaya, D. Howard, D. Hitchcock, P. Puneet, S. Zhu, L. Durham and J. Simpson. Lastly but not least, I would like to thank my closest Clemson friends J. Reid, A. Kayyar, K. Meshinchi,

R. Wadhwa and J. Shi. Thank you all very much for your guidance, mentorship, dedication, patience, support and friendship.

My sincerest gratitude and respect is given to Dr. R. Contreras, Dr. F. Felder, Dr. M. McDonald and Dr. A. Rothenberg for helping me to face and overcome the difficulties I encountered during my journey.

I would like to express my deepest thanks and affection to my family and friends for their emotional support and words of wisdom.

Thank you all very much for your contribution and participation in this important chapter of my life.

## TABLE OF CONTENTS

	Page
<b>TITLE PAGE</b> .....	<i>i</i>
<b>ABSTRACT</b> .....	<i>ii</i>
<b>ACKNOWLEDGMENTS</b> .....	<i>iii</i>
<b>LIST OF TABLES</b> .....	<i>vi</i>
<b>LIST OF FIGURES</b> .....	<i>vii</i>
<b>CHAPTER I: INTRODUCTION</b> .....	1
1.1 Carbon Fibers – General Overview .....	1
1.2 Polyacrylonitrile (PAN) Carbon Fiber .....	6
1.3 Research Objective – Hypothesis .....	11
<b>CHAPTER II: LITERATURE REVIEW</b> .....	14
2.1 Second-Order Elastic Constant – Modulus of Elasticity.....	14
2.2 Higher-Order Elastic Constants (HOECs) .....	20
<b>CHAPTER III: EXPERIMENTAL METHODS</b> .....	25
3.1 Materials: HewTow <sup>®</sup> IM7-12K Carbon Fiber.....	25
3.2 Fiber Puller .....	25
3.3 Equipment Calibration .....	28
3.4 Equipment Automation .....	32
<b>CHAPTER IV: RESULTS AND DISCUSSION</b> .....	36
4.1 Surface Morphology Characterization .....	36
4.2 Elastic Properties .....	37
4.3 Electrical Properties .....	47
4.4 Contribution of epoxy (glue) to the Young’s Modulus of Carbon Fiber .....	50
<b>CHAPTER V: CONCLUSIONS</b> .....	55
<b>CHAPTER VI: RECOMMENDATIONS FOR FUTURE WORK</b> .....	57

## LIST OF TABLES

Table		Page
1.	Values of Young's modulus obtained by both linear and polynomial regression fits for an IM7 sample of gauge length 3.1 mm .....	46

## LIST OF FIGURES

Figure	Page
1. Allotropes of carbon and their structures .....	2
2. Schematic representation of: (a) Well-ordered graphite lattice and, (b) Disordered stacking of interplanar graphite layers .....	3
3. Chemical structures of the acrylonitrile and polyacrylonitrile repeat unit .....	7
4. Conversion of polyacrylonitrile to carbonized carbon fiber after subsequent heat treatments .....	8
5. Methods for determination of Young's modulus with an Instron testing machine.....	10
6. Stress-strain relationship for a single filament of Thornel carbon fiber, after Beetz .....	12
7. Schematic illustration of a body subjected to tensile load .....	14
8. Components of stress tensor in 3D space.....	15
9. Schematic diagram of the fiber puller device .....	26
10. Picture of the fiber puller on a bench top table.....	28
11. Schematic diagram of the force balance in the force-current calibration .....	29
12. $F$ vs. $I$ calibration plot showing a slope of 0.5615 N/A .....	30
13. $C$ vs. $X$ calibration plot showing a slope of 1.42 pF/mV.....	30
14. $1/C$ vs. $\Delta d$ calibration plot .....	31
15. Snapshot of the front panel of the main LabVIEW <sup>®</sup> program used to control the tensile measurements on the fiber puller.....	34

List of Figures (Continued)

Figure	Page
16. SEM image of a single filament of IM7 carbon fiber with diameter of 5.3 microns .....	36
17. Hysteresis loop of five runs of a single filament of the IM7 carbon fiber with the respective sample bow profile for each run .....	39
18. Stress vs. strain pulling plot of an IM7 fiber .....	41
19. Strain vs. stress plot of an IM7 sample .....	42
20. Stress vs. strain % pulling plot of an IM7 sample of gauge length 4.0 mm and $1/V$ vs. strain % correspondent to it .....	44
21. Normalized plots of the $d\sigma/d\varepsilon$ vs. strain % and $1/V$ vs. strain % .....	45
22. Resistance vs. strain plot of an IM7 sample .....	48
23. Hysteresis loop for the resistance vs. strain for the run 15 in Figure 22.....	49

# CHAPTER ONE

## INTRODUCTION

### 1.1 Carbon Fibers – General Overview

Allotropes of carbon include diamond and graphite. Most recently, new forms of carbon such as fullerenes, carbon nanotubes and graphene have been discovered. While diamond and graphite have ordered structures, carbon fibers are usually amorphous. Each form of carbon possesses a unique structure and properties and, in order to be produced, they require specific temperature and pressure treatment conditions. Figure 1 shows the structures of allotropes of carbon.

In graphite the carbon atoms are ordered in a honeycomb plane, with a distance between atoms of 1.42 Å, and the planes are regularly stacked with a spacing of 3.35 Å. The structure of carbon fibers resembles that of graphite but in a more disordered manner, the so called turbostratic structure<sup>1</sup>. Due to the weak nature of the van der Waals forces between the layers, any disorder introduced in the system will affect the interplanar spacing and stacking. Figure 2 is a schematic diagram of the lattices of graphitic (a) and non-graphitic (b) carbons<sup>2</sup>.

---

<sup>1</sup> Thomas W. Ebbesen, *Carbon Nanotubes: Preparation and Properties*, CRC Press, Inc., Boca Raton, FL, 1997.

<sup>2</sup> M. S. Dresselhaus, G. Dresselhaus, P. C. Eklund, *Science of Fullerenes and Carbon Nanotubes*, Academic Press, San Diego, CA, 1996.

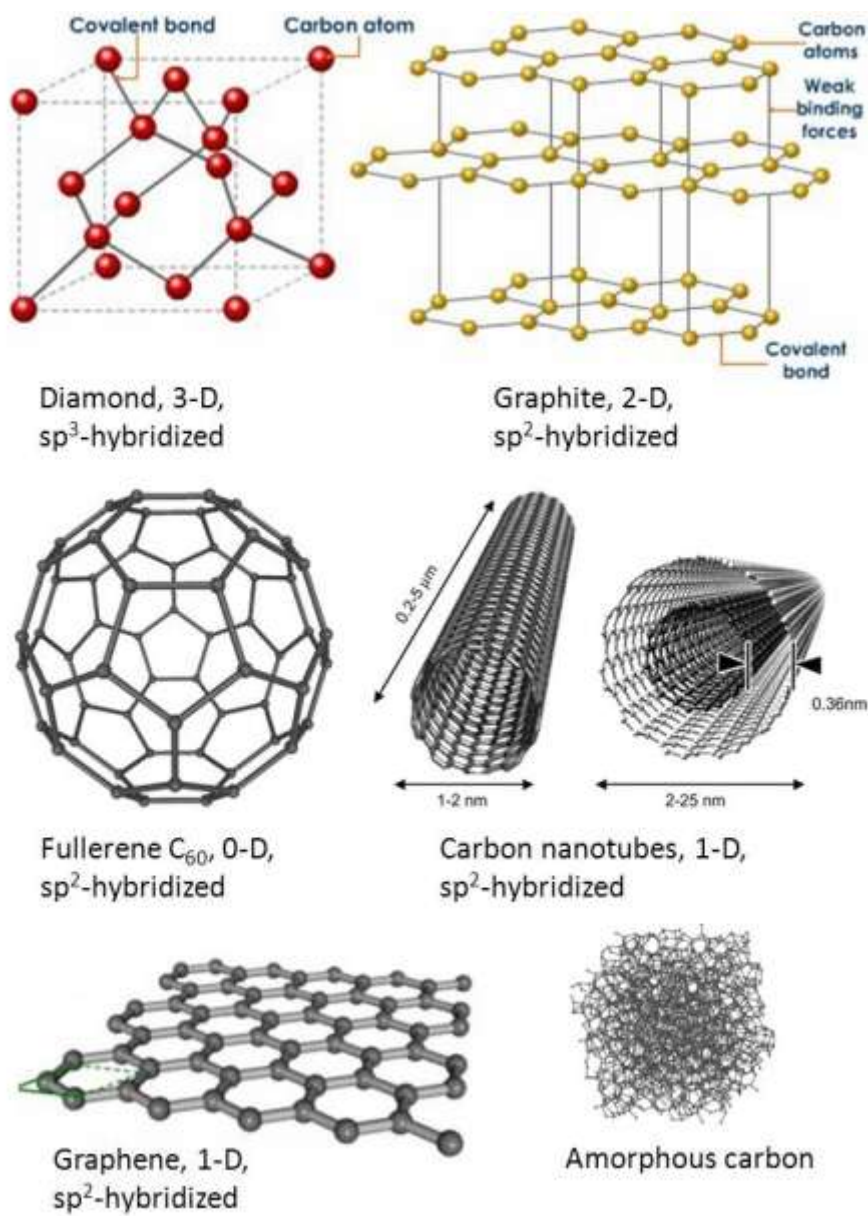


Figure 1. Allotropes of carbon and their structures.

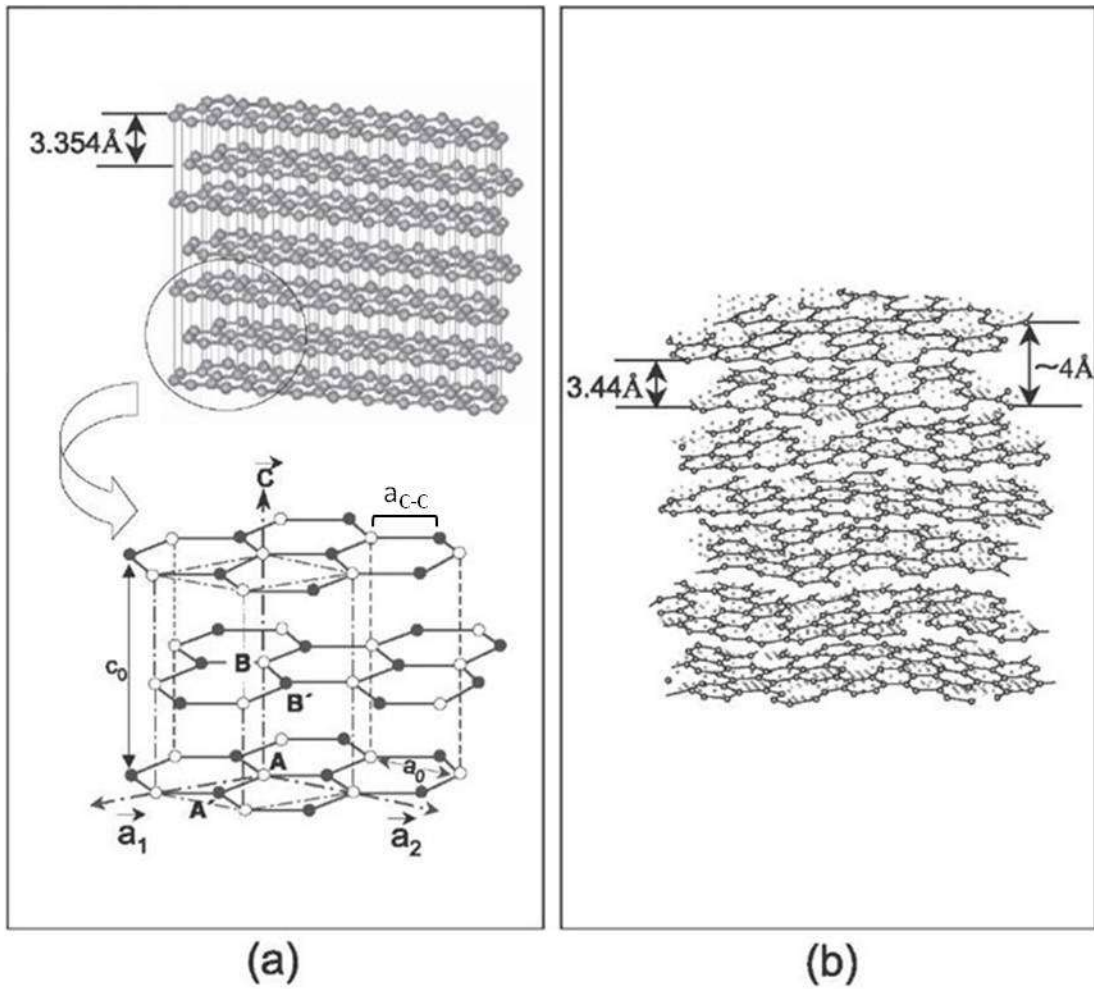


Figure 2. (a) Well-ordered graphite lattice showing its interlayer distance of 3.35 Å. The inset shows A and B carbon atoms represented by open circles and A' and B' carbon atoms represented by closed circles. The nearest neighbor distance between two carbon atoms,  $a_{C-C}$ , in graphite is 1.42 Å. The in-plane lattice constant is represented by  $a_0$  and the unit cell vectors in the direction  $a_1$ ,  $a_2$  and  $c$  are indicated. (b) Disordered stacking of interplanar graphite layers showing random interlayer spacing of at least 3.44 Å<sup>2</sup>.

As can be seen in Figure 1, the tetrahedral bonding nature of the carbon atoms in diamond gives rise to  $sp^3$  hybridization, while in graphite strong covalent bonds exist only between in-plane carbons, giving rise to  $sp^2$  hybridization. The weak van der Waals bonds between the planes are what distinguish the softness of graphite from the hardness of diamond<sup>2</sup>. Carbon materials are known to possess excellent properties, such as: high strength, stiffness, thermal resistance, conductivity and light weight. Diamond has very high modulus of elasticity, and graphite has high moduli for in-planar moduli. Their Young's moduli are reported to be on the order of 1000 GPa<sup>3, 4</sup>. The Young's modulus along the axis of single- and multi-walled carbon nanotubes can range from 1000 - 5000 GPa<sup>5</sup> and their tensile strength from 10 – 60 GPa<sup>6</sup>. Tensile strength is defined as the maximum tensile stress that a specimen can withstand before failure. Carbon fibers can be either graphitic (stronger) or non-graphitic (less strong) depending on the precursor and processing conditions and, therefore, their moduli can approach that of graphite or even diamond.

Knowing that carbon fibers are light materials and also very strong, their commercial use has been made available since the early 60's and has been mainly targeted as a high-performance reinforcement material in several industries, such as: transportation, sporting goods and textiles. Specific applications include: microelectronics, military, aerospace and automotive components, passenger and

---

<sup>3</sup> A. Kelly, N. H. MacMillan, *Strong Solids*, Clarendon Press, Oxford, 3rd Ed., 1986.

<sup>4</sup> J.-P. Salvetat, J.-M. Bonard, N. H. Thomson, A. J. Kulik, L. Forro, W. Benoit, L. Zuppiroli, *Mechanical Properties of Carbon Nanotubes*, Appl. Phys. A **69**, 255-260, 1999.

<sup>5</sup> M. M. J. Treacy, T. W. Ebbesen, J. M. Gibson, *Exceptionally High Young's Modulus Observed for Individual Carbon Nanotubes*, Nature **381**, 678-680, 1996.

<sup>6</sup> M. F. Yu, O. Lourie, M. J. Dyer, K. Moloni, T. F. Kelly, R. S. Ruoff, *Strength and Breaking Mechanism of Multiwalled Carbon Nanotubes Under Tensile Load*, Science **287**, 637-640, 2000.

recreational vehicles, racing cars, and portable consumer goods, such as: bicycle frames, golf club shafts, fishing rods, tennis racquets; novel nanofibers and yarns; etc<sup>7</sup>.

At room temperature and atmospheric pressure graphite is the stable form of carbon as well as the most abundant. Bundy<sup>8</sup> reported the triple point of graphite-diamond, *i. e.*, the point at which vapor, liquid and solid phases are in equilibrium, to be between temperatures of 3700 and 4000 °C and pressures between 12.5 and 13 GPa. It should be noticed that, under industrial processing conditions, it is very difficult and costly to prepare carbon fibers from the liquid phase. For this reason the standard industrial process to obtain them is from organic polymer precursors which are subjected to a three-step heating process<sup>9</sup>:

- 1) Stabilization in air at 300 °C: this stage is responsible for chemical alteration of a linear polymeric chain to a more thermally stable cyclic chain.
- 2) Carbonization at 1100 °C in an inert atmosphere leading to a fiber content of at least 92% carbon: at this stage oxygen is absent from the surroundings and the higher temperatures promote loss of the non-carbon elements in gaseous forms such as water vapor, carbon dioxide, hydrogen and nitrogen.
- 3) Graphitization at temperatures above 2500 °C leading to fibers with carbon in excess of 99%: at this stage the even higher temperatures transform unstable non-graphitic carbons into a more ordered and crystalline graphitic structure.

---

<sup>7</sup> J. B. Donnet, *Carbon Fibers*, Marcel Dekker, Inc. 3<sup>rd</sup> Ed., New York, NY, 1998.

<sup>8</sup> F. P. Bundy, *Melting of Graphite at Very High Pressure*, *Journal of Chemical Physics* **38**, 618-630, 1963.

<sup>9</sup> P. Morgan, *Carbon Fibers and Their Composites*, Taylor & Francis Group, Boca Raton, FL, 2005.

“Graphite fibers” undergo all three steps while “carbon fibers” are not subjected to graphitization.

Based on fiber strength, modulus and final heat treatment, carbon fibers can be classified into different types<sup>9</sup>:

- a) ultra-high modulus (UHM): Young’s modulus > 600 GPa;
- b) high modulus (HM): Young’s modulus > 300 GPa;
- c) intermediate modulus (IM): Young’s modulus between 150 and 300 GPa;
- d) low modulus (LM): Young’s modulus > 100 GPa;
- e) type I, high-heat treatment (HHT): final heat temperature > 2000 °C (related to high-modulus type);
- f) type II, intermediate-heat treatment (IHT): final heat temperature around or above 1000 °C (related to high-strength type);
- g) type III, low-heat treatment (LHT): final heat temperature no higher than 1000 °C (related to low modulus and low-strength type).

The most common precursors for carbon fiber manufacture include: polyacrylonitrile (PAN), rayon (cellulose) and pitch (from petroleum or coal tar). This Thesis will focus on PAN-based carbon fibers which are introduced in the next section.

## **1.2 Polyacrylonitrile (PAN) Carbon Fiber**

Polyacrylonitrile is a linear organic polymer resin obtained from polymerization of acrylonitrile. Both chemical structures are depicted in Figure 3.

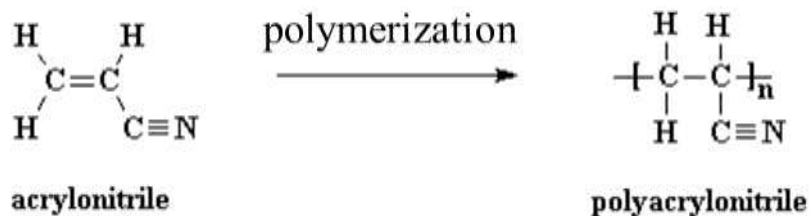


Figure 3. Chemical structures of the acrylonitrile and polyacrylonitrile repeat unit.

PAN-based carbon fibers are non-crystalline fibers obtained from polyacrylonitrile precursors by stabilization, carbonization and final heat treatment. A schematic diagram in Figure 4 shows the conversion of PAN to a carbonized fiber<sup>10</sup>.

About ninety percent of the carbon fiber market is taken by PAN-based fibers<sup>9</sup> due to the affordability of the cheap precursor and the straightforward fabrication process. Their good strength and modulus properties are derived from the preferred orientation of the graphene layers parallel to the fiber axis and also from defects in the structure which prevent the sliding of neighboring planes relative to each other<sup>2</sup>. As previously mentioned, their excellent mechanical properties and light weight are of great interest as reinforcement materials.

The mechanical properties of carbon fibers are usually tested by standard testing procedures for the determination of longitudinal and transverse tensile strength and moduli, longitudinal compression strength and modulus, flexural strength and modulus, and shear strength. Either tow or single-filament fibers can be tested as well as pristine or composite fibers and laminates.

<sup>10</sup> K. Morita, Y. Murata, A. Ishitani, K. Murayama, T. Ono, A. Nakajima, *Characterization of Commercially Available PAN-Based Carbon Fibers*, Pure & Applied Chemistry **58**, 455-468, 1986.

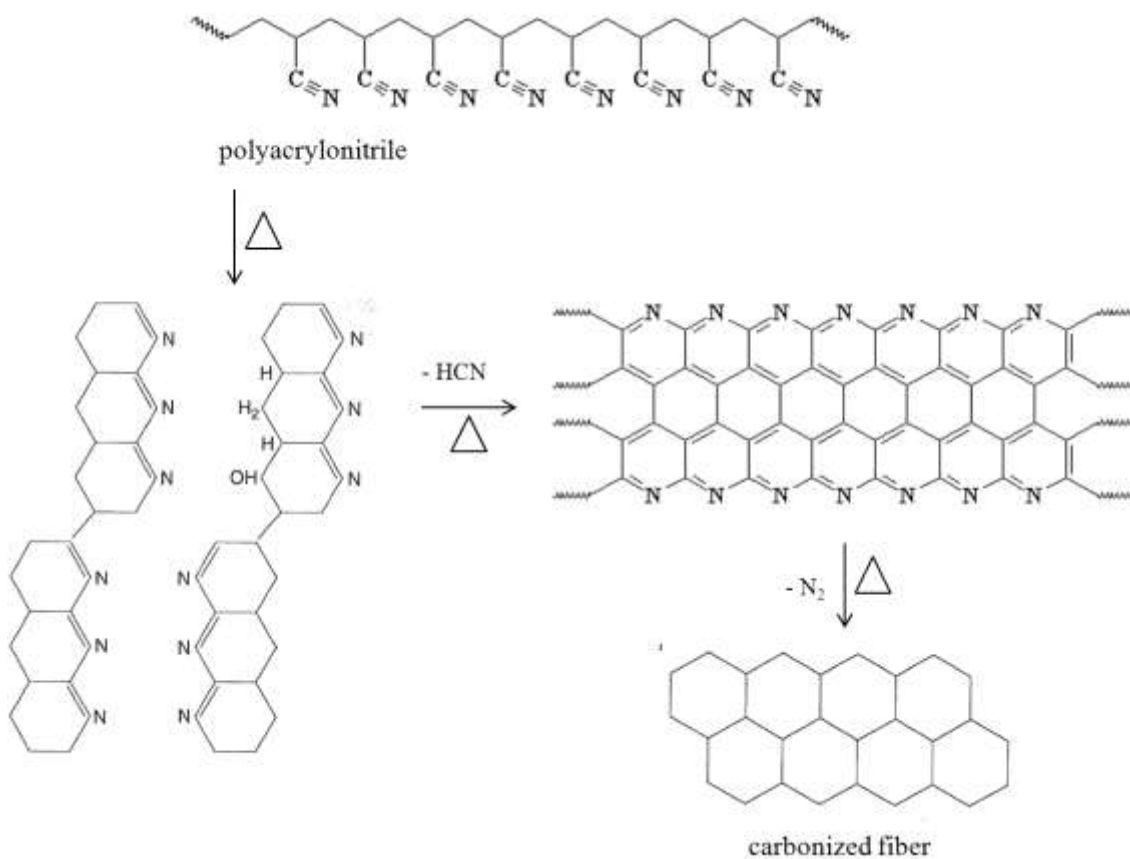


Figure 4. Conversion of polyacrylonitrile to carbonized carbon fiber after subsequent heat treatments<sup>10</sup>.

In the early stages of carbon fiber research all tensile analysis was done by filament testing where only small quantities of samples were needed<sup>9</sup>. After the massive production and commercialization of carbon fibers, testing procedures were designed for analysis of the properties of the tow since the fibers are sold this way and the results correlate better with the properties of composite fibers than those found by the single filament method. When theoretical consideration is carried out, however, it is important to account for the distribution of the tensile strength of single filament fibers<sup>10</sup>.

Mechanical properties are normally measured using a universal testing machine which is capable of performing either tensile or compressive tests. From tensile measurements, tensile strength and maximum elongation can be determined as well as Young's modulus.

The most common testing equipment is the Instron machine. The specimen to be tested must have specific dimensions and the testing machine should have been completely leveled, aligned axially and carefully calibrated. The carbon fiber, in this case, is mounted in a cardboard holder, the ends of the fiber are usually glued with epoxy and the cardboard is placed between two grips. Prior to testing, the sides of the holder are cut so only the fiber is tensed. The force applied to the sample is measured by a load cell as a movable cross-head at a constant speed elongates the sample until it breaks. The machine is equipped with software that calculates modulus and tensile strength as well as other properties depending on the standard method chosen for analysis. The software can calculate the modulus using different methods as shown in Figure 5<sup>9</sup> and it is important to know which method was established for modulus determination.

Extensive research has been done on the mechanical properties of carbon fibers and, since the Instron machine is very popular, attention is not given to the data produced more than it is to the readily available Young's modulus value that the software generates. Mostly known as the slope of the stress-strain plot, Young's modulus is usually calculated taking into account only the linear fit to the plot and neglecting the curvature or, according to other methods, the entire data set of the plot is not taken into consideration. This will give rise to deviations of the measured Young's modulus from the standard thermodynamic definition, as shown below.

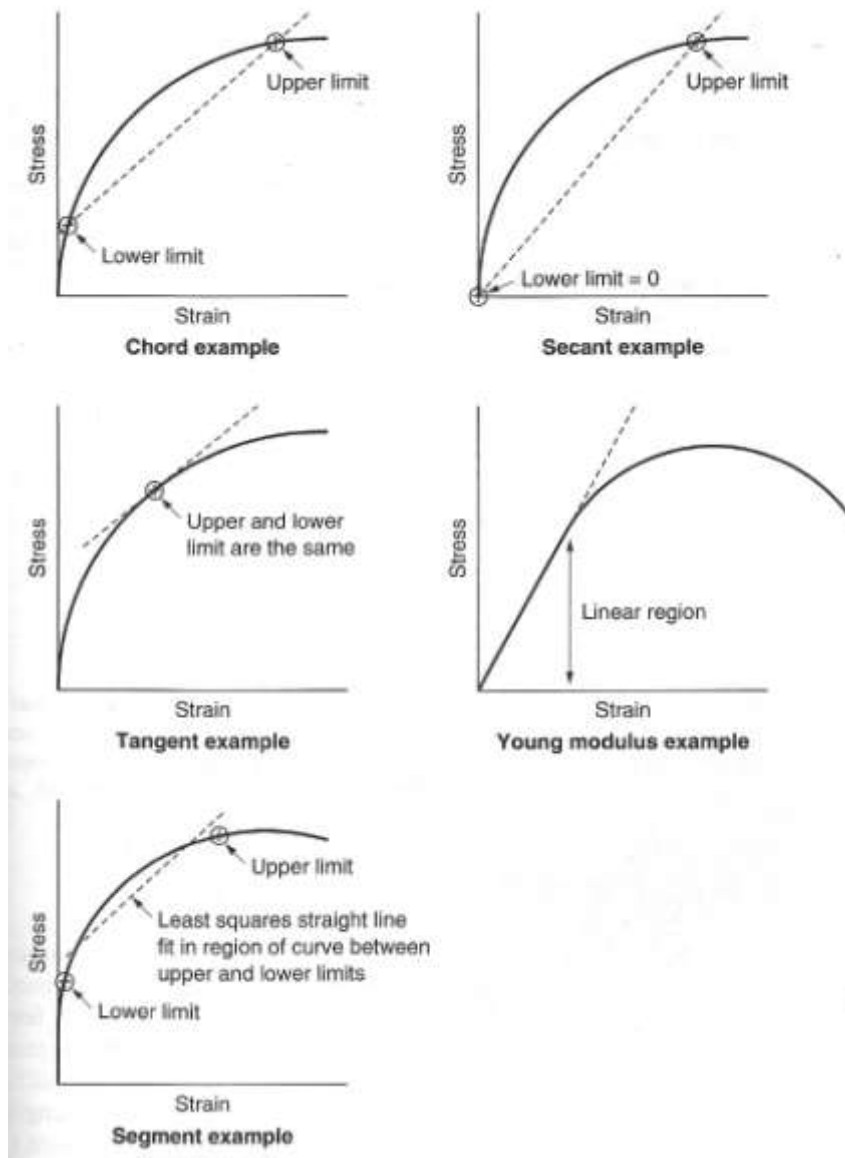


Figure 5. Methods for determination of Young's modulus with an Instron testing machine<sup>9</sup>.

Although many studies establish linear elasticity for carbon fibers due to a seeming linear stress-strain relationship at the traditional rates of elongation, carbon fibers from rayon or PAN precursors have shown nonlinear elastic behavior according to previous reports in the literature<sup>11, 12, 13, 14, 15</sup>. High tensile strength fibers undergo stiffening under load and, therefore, do not obey Hooke's law<sup>15</sup>.

Beetz<sup>14</sup> investigated the strain-induced stiffening of carbon fibers and, like other researchers, he focused on the mechanism of deformation which led to the observation of nonlinear elasticity. Figure 6 shows the stress-strain relation of a single filament of Thornel carbon fiber subjected to tensile testing using an Instron machine<sup>14</sup>. It is explained that, due to stiffening, an initial and final modulus can be obtained. Small strains at the initial stage give rise to lower slopes and, just before failure, a final slope with a higher value is obtained.

### 1.3 Research Objective – Hypothesis

It is well known that carbon fibers possess excellent mechanical properties and for this reason are of great interest as reinforcement materials. The elastic properties of carbon materials have been extensively investigated as well as carbon fiber composites.

---

<sup>11</sup> G. J. Curtis, J. M. Milne, W. N. Reynolds, *Non-Hookean Behavior of Strong Carbon Fibers*, Nature **220**, 1024-1025, 1968.

<sup>12</sup> A. Voet, J. C. Morawski, J. B. Donnet, *Dynamic Mechanical Properties of Carbon Fibers*, Carbon **13**, 465-468, 1975.

<sup>13</sup> A. Gupta, I. R. Harrison, *New Aspects in the Oxidative Stabilization of PAN-based Carbon Fibers: II*, Carbon **35**, 809-818, 1997.

<sup>14</sup> C. P. Beetz, Jr., *Strain-Induced Stiffening of Carbon Fibers*, Fibre Science and Technology **16**, 219-229, 1982.

<sup>15</sup> M. Guigon, A. Oberlin, G. Desarmot, *Microtexture and Structure of High Tensile Strength PAN-based Carbon Fibers*, Fibre Science and Technology **20**, 55-72, 1984.

Advancements in technology have forced the development of even stronger carbon fibers in order to meet the demand in novel applications. The current state-of-the-art does not pay much attention to the non-Hookean behavior of strong carbon fibers when determining their elastic properties as well as of their composites. The nonlinear elastic behavior of strong carbon fibers is indicative of the presence of higher-order elastic constants other than the modulus of elasticity measured by the average slope of a stress-strain curve.

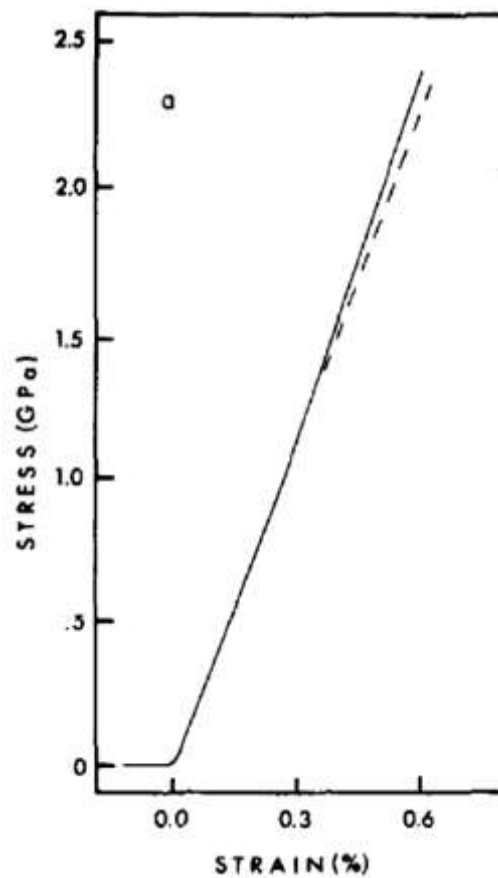


Figure 6. Stress-strain relationship for a single filament of Thornel carbon fiber, after Beetz. The dashed line is an extrapolation of the initial linear portion of the curve<sup>14</sup>.

A universal testing machine equipped with software that can calculate a material's Young's modulus using different methods is popular among researchers, however, the entire data set obtained during testing is often not considered when calculating the material's modulus of elasticity leading to a less useful measurement of this important property.

The objective of this research was to measure the usual second-order elastic constant (Young's modulus) as well as the nonlinearity constant  $\delta$ , which is a combination of third-order elastic constants, of a single filament of HewTow<sup>®</sup> IM7-12K PAN-based carbon fibers. A fiber puller specifically designed and built to accommodate micro scale size samples was employed. A LabVIEW<sup>®</sup> software program was developed to control the experiments and a second lock-in amplifier was employed to measure the slope of the stress-strain curve directly. IM7 carbon fiber is a PAN-based carbon fiber of intermediate modulus. Performance of tensile tests was expected to reveal non-Hookean behavior of IM7, since it is a relatively high strength material. No reference to the higher-order elastic constant of a single filament of IM7 was found in the literature.

## CHAPTER TWO

### LITERATURE REVIEW

#### 2.1 Second-Order Elastic Constant – Modulus of Elasticity

Engineering stress,  $\sigma$  (in MPa) is defined as:

$$\sigma = \frac{F}{A} \quad (1)$$

where,  $F$  (in N) is the load applied perpendicular to a sample's cross-section and,  $A$  (in  $\text{m}^2$ ) is the material's cross-section area before load is applied<sup>16</sup>. Engineering strain,  $\varepsilon$  (dimensionless) is defined as:

$$\varepsilon = \frac{l - l_0}{l_0} \quad (2)$$

where,  $l$  is the specimen's length after elongation and,  $l_0$  is the initial length before load is applied<sup>16</sup>.

A schematic illustration of a body subjected to tensile load is depicted in Figure 7.

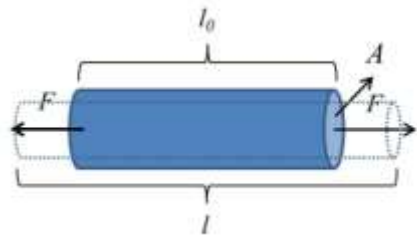


Figure 7. Schematic illustration of a body subjected to tensile load. The dashed lines indicate the shape of the specimen after elongation.

<sup>16</sup> W. D. Callister, Jr., *Materials Science and Engineering: An Introduction*, John Wiley and Sons, 6<sup>th</sup> Ed., Hoboken, NJ, 2003.

No crystals have a Young's modulus that is the same in all directions. Consider Figure 8 below which displays the spatial orientation components of a 3D differential element. Plane directions are described as x, y and z and the stress components in each direction are also displayed.

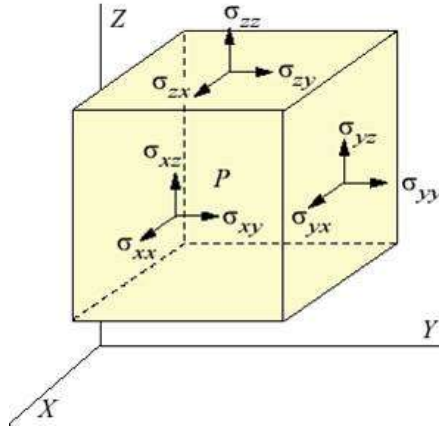


Figure 8. Components of stress tensor in 3D space.

Under static equilibrium, the stress state at a point P is described by a second-order stress tensor of nine components associated with two directions (x, y, z) or (1, 2, 3) as shown below. As a result, stress components have two subscripts<sup>17</sup>.

$$\begin{pmatrix} \sigma_{xx} & \sigma_{xy} & \sigma_{xz} \\ \sigma_{yx} & \sigma_{yy} & \sigma_{yz} \\ \sigma_{zx} & \sigma_{zy} & \sigma_{zz} \end{pmatrix} \Rightarrow \sigma_{ij} = \begin{pmatrix} \sigma_{11} & \sigma_{12} & \sigma_{13} \\ \sigma_{21} & \sigma_{22} & \sigma_{23} \\ \sigma_{31} & \sigma_{32} & \sigma_{33} \end{pmatrix}$$

where,  $\sigma_{ij}$  represents the stress on the  $i$  plane along the  $j$  direction;  $i$  is the direction of the surface normal upon which the stress acts,  $j$  is the direction of the stress component and,  $i, j = 1, 2, 3$  are component indices.

<sup>17</sup> J. F. Nye, *Physical Properties of Crystals: Their Representation by Tensors and Matrices*, Oxford University Press, London, UK, 1957.

Similarly, strain tensors follow a similar rule as shown below:

$$\varepsilon_{ij} = \begin{pmatrix} \varepsilon_{11} & \varepsilon_{12} & \varepsilon_{13} \\ \varepsilon_{21} & \varepsilon_{22} & \varepsilon_{23} \\ \varepsilon_{31} & \varepsilon_{32} & \varepsilon_{33} \end{pmatrix}$$

Tensor notation indices 11, 22, 33, 23 and 32, 31 and 13, 12 and 21 for the stress  $\sigma_{ij}$  can be reduced to 1, 2, 3, 4, 5 and 6, respectively, in matrix (Voigt) notation. This is due to the diagonal symmetry of the tensors, which in turn is due to the constraints of no motion (for stress) and the definition of the strains, as below. The resultant stress matrix is<sup>17</sup>:

$$\begin{pmatrix} \sigma_1 & \sigma_6 & \sigma_5 \\ \sigma_6 & \sigma_2 & \sigma_4 \\ \sigma_5 & \sigma_4 & \sigma_3 \end{pmatrix}$$

The strain tensor  $[\varepsilon_{ij}]$  is the symmetrical part of  $[e_{ij}]$ , where  $e_{ij}$  is defined as the strain at the point  $P$ :

$$\varepsilon_{ij} = \frac{1}{2} (e_{ij} + e_{ji}) = \varepsilon_{ji} \quad (3)$$

$$e_{ij} = \frac{\partial u_i}{\partial x_j} \quad (4)$$

where  $\partial u$  is the increase in length and  $\partial x$  is the differential change in length. Utilizing the identity equation in (3) the strain tensor is reduced to the matrix notation below:

$$\begin{pmatrix} \varepsilon_{11} & \varepsilon_{12} & \varepsilon_{13} \\ \varepsilon_{21} & \varepsilon_{22} & \varepsilon_{23} \\ \varepsilon_{31} & \varepsilon_{32} & \varepsilon_{33} \end{pmatrix} \rightarrow \begin{pmatrix} \varepsilon_{11} & \frac{1}{2}(e_{12} + e_{21}) & \frac{1}{2}(e_{13} + e_{31}) \\ \frac{1}{2}(e_{12} + e_{21}) & \varepsilon_{22} & \frac{1}{2}(e_{23} + e_{32}) \\ \frac{1}{2}(e_{13} + e_{31}) & \frac{1}{2}(e_{23} + e_{32}) & \varepsilon_{33} \end{pmatrix} \rightarrow \begin{pmatrix} \varepsilon_1 & \frac{1}{2}\varepsilon_6 & \frac{1}{2}\varepsilon_5 \\ \frac{1}{2}\varepsilon_6 & \varepsilon_2 & \frac{1}{2}\varepsilon_4 \\ \frac{1}{2}\varepsilon_5 & \frac{1}{2}\varepsilon_4 & \varepsilon_3 \end{pmatrix}$$

The principal tensile strains resultant from stretching,  $\varepsilon_1$ ,  $\varepsilon_2$  and  $\varepsilon_3$ , are the diagonal components of  $\varepsilon_{ij}$  and the other components,  $\varepsilon_4$ ,  $\varepsilon_5$  and  $\varepsilon_6$ , measure shear strains resultant from parallel or tangent forces applied to the surface of the material.

An isotropic material is identical in all directions and its properties are not dependent on directionality. In this case, its modulus of elasticity, or Young's modulus  $E$  is the same for all directions when such a material is subjected to any tension or compression. The linear theory of elasticity<sup>18</sup> states that strain  $\varepsilon$  is proportional to stress  $\sigma$ , so that a straight line is obtained in a stress *versus* strain plot. As long as the forces applied to the body are proportional to the resulting strains, the body obeys Hooke's law. In this case, the stress-strain relation can be written as:

$$\sigma = E \varepsilon \quad (5)$$

Anisotropic materials, however, have properties that differ according to the direction of measurement. For anisotropic elastic materials, the stress-strain relations can be written as<sup>17</sup>:

$$\sigma_{ii} = C_{ijj} \varepsilon_{jj} \quad (6)$$

$$\varepsilon_{ii} = S_{ijj} \sigma_{jj} \quad (7)$$

where,  $\varepsilon_{ii}$  is the  $ii^{th}$  component of a second-rank strain tensor;  $\sigma_{ii}$  is the  $ii^{th}$  component of a second-rank stress tensor;  $C_{ijj}$  is the elastic stiffness tensor,  $S_{ijj}$  is the elastic compliance tensor, and the Einstein sum convention, in which subscripts that are repeated two or more times in a product are summed, is used. Both  $C_{ijj}$  and  $S_{ijj}$  are the  $ijj^{th}$  components of fourth-rank tensors with 81 components, each necessary to connect two second-rank

---

<sup>18</sup> A. I. Lurie, *Theory of Elasticity*. Springer, Netherlands, 2005.

tensors, the stress and strain tensors. The elastic compliance  $S$  is the inverse of Young's modulus,  $1/E$ .

Considering equation (7) written out for  $\varepsilon_{11}$  we have:

$$\begin{aligned} \varepsilon_{11} = & S_{1111} \sigma_{11} + S_{1112} \sigma_{12} + S_{1113} \sigma_{13} + \\ & S_{1121} \sigma_{21} + S_{1122} \sigma_{22} + S_{1123} \sigma_{23} + \\ & S_{1131} \sigma_{31} + S_{1132} \sigma_{32} + S_{1133} \sigma_{33} \end{aligned} \quad (8)$$

In the matrix notation equation (8) becomes:

$$\begin{aligned} \varepsilon_1 = & S_{11} \sigma_1 + \frac{1}{2} S_{16} \sigma_6 + \frac{1}{2} S_{15} \sigma_5 \\ & + \frac{1}{2} S_{16} \sigma_6 + S_{12} \sigma_2 + \frac{1}{2} S_{14} \sigma_4 \\ & + \frac{1}{2} S_{15} \sigma_5 + \frac{1}{2} S_{14} \sigma_4 + S_{13} \sigma_3 \end{aligned} \quad (9)$$

In general, the equation takes the shorter form:

$$\varepsilon_i = s_{ij} \sigma_j \quad (10)$$

where:  $i, j = 1, 2, \dots, 6$ , and the Einstein convention is used.

Young's modulus denotes the slope of the stress-strain curve in uniaxial tension, and has the dimensions of stress,  $\text{N/m}^2$  or GPa. Poisson's ratio,  $\nu$ , is the ratio of the lateral to longitudinal strain in a uniaxial tensile stress, and it is a dimensionless quantity. Young's modulus and Poisson's ratio vary with direction in a non-isotropic solid, and are a function of direction in anisotropic materials, such as IM7 carbon fiber. In an isotropic material, any two of  $E$ ,  $\nu$ , and  $G$  (the shear modulus), determine the material's linear elasticity. The shear modulus, or modulus of rigidity, is defined as the ratio between the shearing stress that deforms a material in the lateral direction and the shearing strain produced by this stress.

Carbon fibers are generally only transversely isotropic, in which Young's modulus depends only on the angle with respect to the axial direction. A complete

description of the linear elasticity of such a substance requires five engineering constants<sup>19</sup>: axial Young's modulus ( $E_{11}$ ), shear modulus ( $G_{11}$ ), transverse Young's modulus ( $E_{22}$ ), transverse shear modulus ( $G_{22}$ ) and axial Poisson's ratio ( $\nu_{12}$ ). In terms of the five independent compliance constants ( $S_{ij}$ ) they are:  $S_{11}$ ,  $S_{12}$ ,  $S_{13}$ ,  $S_{33}$  and  $S_{44}$ . Equations 11 to 15 show the relationship between the engineering and elastic compliance constants<sup>19</sup>.

$$S_{11} = \frac{1}{E_1} \quad (11)$$

$$S_{12} = -\frac{\nu_{12}}{E_1} \quad (12)$$

$$S_{13} = -\frac{\nu_{13}}{E_1} \quad (13)$$

$$S_{33} = \frac{1}{E_3} \quad (14)$$

$$S_{44} = \frac{1}{G_{13}} \quad (15)$$

This Thesis shows the results measured for one combination. The constants related to linear behavior, such as Young's modulus and Poisson's ratio are called the second-order elastic constants, as they are given by second derivatives of a thermodynamic potential of the substance<sup>20</sup>. If the isothermal  $E$  is defined as the second derivative of the Gibbs energy with respect to stress, evaluated at zero stress, then it is

---

<sup>19</sup> M. Cheng, W. Chen, *Mechanical Properties of Kevlar<sup>®</sup> KM2 Single Fiber*, Journal of Engineering Materials and Technology **127**, 197-203, 2005.

<sup>20</sup> K. Brugger, *Thermodynamic Definition of Higher-Order Elastic Coefficients*, Physical Review **133**, A1611-A1612, 1964.

determined by the linear term in a fit to a stress-strain curve taken at constant temperature.

The nonlinear properties are related to higher-order derivatives of thermodynamic potentials. An isotropic material requires three third-order elastic constants to completely describe the third-order behavior, and a material with transverse isotropic symmetry, such as IM7 carbon fibers, requires nine<sup>21</sup> of which we have measured one combination of six. The concept of higher-order elastic constants is introduced in the following section.

## 2.2 Higher-Order Elastic Constants (HOECs)

In order to design novel reinforced carbon composite materials, for instance, carbon fiber and carbon nanotube composites, it is important to consider the known properties of the pristine carbon material and the matrix individually in the initial stage of the composite design. Using the knowledge of the elastic properties of the materials incorporated into composites, one can model and calculate a set of elastic constants as well as simulate their behavior under specific working circumstances<sup>9</sup>.

At a high enough strains and stresses, deviations from Hooke's law will occur. The nonlinear theory of elasticity of materials is more complex and leads to the introduction of HOECs. The investigation of HOECs is important in determining the anharmonic properties of materials such as: nonlinear elasticity, thermal conductivity and

---

<sup>21</sup> I. J. Fritz, *Third-Order Elastic Constants for Materials with Transversely Isotropic Symmetry*, Journal of Applied Physics **48**, 812-814, 1977.

thermal expansion, solid-state diffusion, static and dynamic properties of lattice defects and phonon-phonon interactions<sup>22</sup>.

Nonlinear elasticity<sup>23</sup> is generally apparent when large deformations are applied, and usually when the sample is on the micro or nano scale. HOECs can be expressed in the form<sup>24</sup>:

$$\varepsilon_I = s_{11} \sigma_I + \delta (s_{11} \sigma_I)^2 \quad (16)$$

where:  $\varepsilon_I$  is the strain,  $\sigma_I$  is the stress,  $s_{11}$  is an elastic constant and,  $\delta$  is a nonlinearity constant (a combination of second- and third-order elastic constants).

Riley and Skove<sup>25</sup> have shown how to determine the relation between  $\delta$  and the third-order elastic constants for various directions in substances of arbitrary symmetry. For stress along the symmetry axis of a transversely isotropic substance the relation is:

$$\delta_{001} = 2 s_{133} (C_{111} + 3 C_{112}) + 6 s_{13} s_{33} (s_{13} C_{113} + s_{13} C_{123} + s_{33} C_{133}) + s_{333} C_{333} \quad (17)$$

Although the properties of macro-scale materials are well established today, it is still not completely known how bulk materials made of nanostructures, or how nanostructures by themselves, will behave under large strains and stresses and, therefore, it may be important to know their anharmonicity. Their anharmonic nature originates from the changes in interatomic forces due to atomic displacements<sup>26</sup>.

---

<sup>22</sup> Y. Hiki, *Higher Order Elastic Constants of Solids*. Ann. Rev. Mater. Sci. **11**, 51-73, 1981.

<sup>23</sup> M. A. Biot, *Nonlinear Theory of Elasticity and the Linearized Case for a Body Under Initial Stress*. Philosophical Magazine, Ser. 7, Vol. 27, Columbia University, 1939.

<sup>24</sup> F. D. Murnaghan, *Finite Deformation of an Elastic Solid*, Dover Publications, New York, 1967.

<sup>25</sup> M. W. Riley, M. J. Skove, *Higher-Order Elastic Constants of Copper and Nickel Whiskers*, Physical Review B **8**, 466-474, 1973.

<sup>26</sup> A. G.-Comas, L. Manosa, A. Planes, M. Morin, *Anharmonicity of Cu-based Shape-Memory Alloys in the Vicinity of their Martensitic Transition*, Physical Review B **59**, 246-250, 1999.

Elastic properties of materials have been determined in different ways. Both experimental and theoretical approaches have been used. Besides the universal testing machine for experimental determination of second-order elastic constants<sup>13, 14, 15, 27, 28</sup>, elastic moduli can also be measured dynamically by oscillatory forces applied at very small amplitudes to statically stretched fibers<sup>12</sup>. HOECs can furthermore be determined by acoustical measurements<sup>11, 29, 30 31</sup> which generally determine more combinations of constants, since each polarization of the wave determines a different combination. Bogardus<sup>32</sup> utilized a pulse superposition method to determine the ultrasonic velocity as a function of both uniaxial and hydrostatic pressure of germanium, magnesium oxide, and fused silica.

Recently, Segur *et al.*<sup>33</sup> used a pump-probe technique to generate acoustic waves and propagate them in the cross-section of micrometric single carbon fibers in order to measure their elastic properties in the transverse direction as well as the fiber's optical properties. The researchers studied two different carbon fibers and found that their elastic coefficients  $c_{11}$  were in the same range of order,  $30 \pm 6$  GPa for a low elastic modulus carbon fiber and  $15 \pm 3$  GPa for a high elastic modulus PAN-based carbon fiber;

---

<sup>27</sup> T. H. Ko, *Influence of Continuous Stabilization on the Physical Properties and Microstructure of PAN-based Carbon Fibers*, Journal of Applied Polymer Science **42**, 1949-1957, 1991.

<sup>28</sup> M. C. Paiva, C. A. Bernardo, M. Nardin, *Mechanical, Surface and Interfacial Characterization of Pitch and PAN-based Carbon Fibers*, Carbon **38**, 1323-1337, 2000.

<sup>29</sup> E. H. Bogardus, *Temperature Dependence of the Pressure Coefficients of Elastic Constants for NaCl*, Journal of Applied Physics **36**, 3544-3546, 1965.

<sup>30</sup> W. H. Prosser, R. E. Green, Jr., *Characterization of the Nonlinear Elastic Properties of Graphite/Epoxy Composites Using Ultrasound*, Journal of Reinforced Plastics and Composites **9**, 162-173, 1990.

<sup>31</sup> R. E. Smith, *Ultrasonic Elastic Constants of Carbon Fibers and their Composites*, Journal of Applied Physics **43**, 2555-2561, 1972.

<sup>32</sup> E. H. Bogardus, *Third-Order Elastic Constants of Ge, MgO, and Fused SiO<sub>2</sub>*. Journal of Applied Physics **36**, 2504-2513, 1965.

<sup>33</sup> D. Segur, Y. Guillet, B. Audoin, *Picosecond Ultrasonics on a Single Micron Carbon Fiber*. J. Phys. **278**, 012020-1-4, 2011.

however, their elastic moduli  $E$  in the axial direction were considerably different (53 GPa for the low modulus and 380 GPa for the PAN-based carbon fiber) due to their dissimilar microstructure. A device similar to that used in this Thesis has been previously used to determine the combinations of HOECs of a set of different materials – Cu and Ni<sup>25</sup>, Pb<sup>34</sup>, Al<sup>35</sup>, Zn and Cd<sup>36</sup>, fused quartz<sup>37</sup> and, Fe and Ag whiskers<sup>38</sup> – using finite deformations. Their method has shown results that are in good agreement, experimentally and theoretically, with results from the literature.

Further, simulations and first principle calculations are often made for carbon materials as well as their composites. Theoretical modeling is of great interest so that composite properties can be characterized for potential engineering applications. Physical constants of nonlinear elastic fibrous micro and nano composites have been predicted by Cattani *et al.*<sup>39</sup>; Naik *et al.*<sup>40</sup> have formulated a model for determination of the elastic properties of impregnated twisted yarns made of long unbroken filaments; Hlavacek *et al.*<sup>41</sup> have calculated the elastic stiffness constants of unidirectional fiber-reinforced composites with a hexagonal layout of fibers using the effective stiffness

---

<sup>34</sup> B. E. Powell, M. J. Skove, *Combinations of Third-Order Elastic Constants of Lead*, Journal of Applied Physics **51**, 3433-3434, 1980.

<sup>35</sup> B. E. Powell, M. J. Skove, *A Combination of Third-Order Elastic Constants of Aluminum*, Journal of Applied Physics **53**, 764-765, 1982.

<sup>36</sup> B. E. Powell, M. J. Skove, *Combinations of Third-Order Elastic Constants of Zinc and Cadmium*, Journal of Applied Physics **44**, 666-667, 1973.

<sup>37</sup> B. E. Powell, M. J. Skove, *Combinations of Fourth-Order Elastic Constants of Fused Quartz*, Journal of Applied Physics **41**, 4913-4917, 1970.

<sup>38</sup> B. E. Powell, M. J. Skove, *Measurement of Higher-Order Elastic Constants Using Finite Deformations*, Phys. Rev. **174**, 977-983, 1968.

<sup>39</sup> C. Cattani, J. J. Rushchitsky, S. V. Sinchilo, *Physical Constants for One Type of Nonlinearly Elastic Fibrous Micro- and Nanocomposites with Hard and Soft Nonlinearities*. Int. Appl. Mech. **41**, 1368-1377, 2005.

<sup>40</sup> N. K. Naik, V. Madhavan, *Twisted Impregnated Yarns: Elastic Properties*. J. Strain Analysis **35**, 83-91, 2000.

<sup>41</sup> M. Hlavacek, *A Continuum Theory for Fibre Reinforced Composites*, International Journal of Solids and Structures **11**, 199-211, 1975.

theory developed by Sun *et al.*<sup>42</sup>; Datta *et al.*<sup>43</sup> used a multiple-scattering approach to derive the effective elastic constants of an anisotropic graphite fiber-reinforced epoxy composite; Thissell *et al.*<sup>44</sup> calculated the elastic properties of polycrystalline anisotropic fibers of cylindrical symmetry and porosity using a preferred orientation model called the “Tomé ellipsoidal self-consistent model”. The researchers compared their results with those “back calculated” from a composite laminate made of a PAN-based carbon fiber and epoxy using the Halpin-Tsai model and found significant differences between the two results. They attributed these differences to the fact that the Halpin-Tsai model was developed using isotropic reinforcement materials and is not directly applicable to cases of anisotropic materials.

One of the objectives of this study was to measure HOECs of a single filament of HewTow<sup>®</sup> IM7-12K carbon fibers. No reference to the HOECs of a single filament of IM7 was found in the literature. Comparison between the outcomes of this work and theoretical results will aid in better understanding these materials as well as their composites.

---

<sup>42</sup> C. T. Sun, J. D. Achenbach, G. Herrmann, *Continuum Theory for a Laminated Medium*, Journal of Applied Mechanics **35**, 467-475, 1968.

<sup>43</sup> S. K. Datta, H. M. Ledbetter, R. D. Kriz, *Calculated Elastic Constants of Composites Containing Anisotropic Fibers*, International Journal of Solids and Structures **20**, 429-438, 1984.

<sup>44</sup> W. R. Thissell, A. K. Zurek, F. Addessio, *Accurate Estimation of the Elastic Properties of Porous Fibers*, 11<sup>th</sup> International Conference on Composite Materials, Gold Coast, Australia, 1997.

## CHAPTER THREE

### EXPERIMENTAL METHODS

#### 3.1 Materials: HewTow<sup>®</sup> IM7-12K Carbon Fiber

A HewTow<sup>®</sup> IM7-12K carbon fiber tow was provided by the Hexcel Corp., Stamford, Connecticut (lot # 5023-10M). The fiber tow is comprised of approximately 12,000 cylindrical filaments of continuous, PAN-based carbon fibers of high performance and intermediate modulus. The measurements were performed using single filaments of the tow which were separated using tweezers and an optical microscope. In order to verify the filament diameter reported by the manufacturer, the surface morphology was characterized and the diameter measured using a field emission scanning electron microscope (SEM), model Hitachi S4800. Samples with gauge lengths ranging from 2.2 to 5.5 mm were tested as-received at room temperature.

#### 3.2 Fiber Puller

The tensile experiments were performed in an instrument specifically designed and built to test micro scale size samples. A schematic diagram of the bench sized puller device is shown in Figure 9, which is described in detail elsewhere<sup>45</sup>.

---

<sup>45</sup> M. J. Skove, T. M. Tritt, A. C. Ehrlich, H. S. Davis, *Device for Simultaneously Measuring Stress, Strain and Resistance in Whiskerlike Materials in the Temperature Range 1.5 K < T < 360 K*, Review of Scientific Instruments **62**, 1010-1014, 1991.

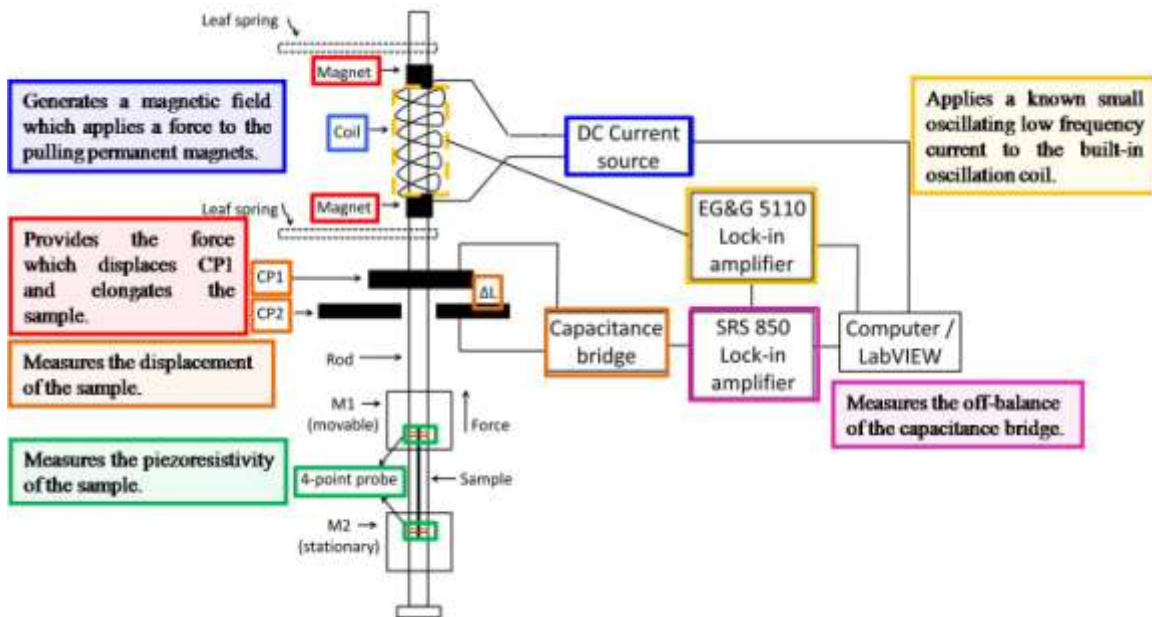


Figure 9. Schematic diagram of the fiber puller device.

The fiber puller capabilities are several: tensile measurements can determine tensile strength, maximum elongation at failure, and tensile modulus of micro-scale samples with diameters ranging from 1 to 100 microns and lengths from ~0.5 to 7 mm. The instrument is also capable of determining resistivity, piezoresistivity and cyclic mechanical and electrical behavior based on hysteresis studies. The coupling of a second lock-in amplifier to the equipment allows real-time verification of nonlinearities in the stress-strain relations. Temperature dependent studies in the range between 1.5 and 360 Kelvin can also be performed, since the equipment is constructed so that it can be inserted in a Janis Vari-temp Dewar, although all data presented here were taken at room temperature. The fiber puller operation is described briefly below.

A current provides a magnetic field which is applied to built-in permanent magnets. The resulting force elongates the sample and displaces the capacitor plate (CP1) that moves with the sample. The resulting change in capacitance is used to determine the elongation of the sample. The fiber filament was secured at both ends using Devcon<sup>®</sup> S-31 or S-6 high-strength weld epoxy. The puller device is connected to a power supply which provides the magnet current, a capacitance bridge which measures the capacitance, a lock-in amplifier (SRS 850) which measures the off-balance of the capacitance bridge, and a computer system which collects the data obtained using a LabVIEW<sup>®</sup> program. To measure the piezoresistivity, a four-point probe was set up with two copper wire pairs placed on each of the mounting plates (M1, M2) and contacts made to the fiber with silver paint. The wires are electrically connected to a multimeter which is also connected to the computer system. A second lock-in amplifier (EG&G 5110) was added to the entire device setup with the role of applying a known small oscillating low frequency (approximately 5 – 20 Hz) current to the oscillating coils. The resulting oscillation in the length of the sample causes an oscillation in the capacitance which is measured by the second lock-in. This is too fast for most damping and creep mechanisms for the sample to respond, so that only the elastic properties are usually seen. The amplitude of this oscillation is inversely proportional to the slope of the stress-strain curve. The resulting data obtained from it was used to check the second derivative  $d^2\sigma/d\varepsilon^2$  during pulling.

A picture of the fiber puller is shown in Figure 10. To appreciate how small the stress-strain device is a blue square has been placed in the picture. The mounting plates M1 and M2 are shown inside a red square.

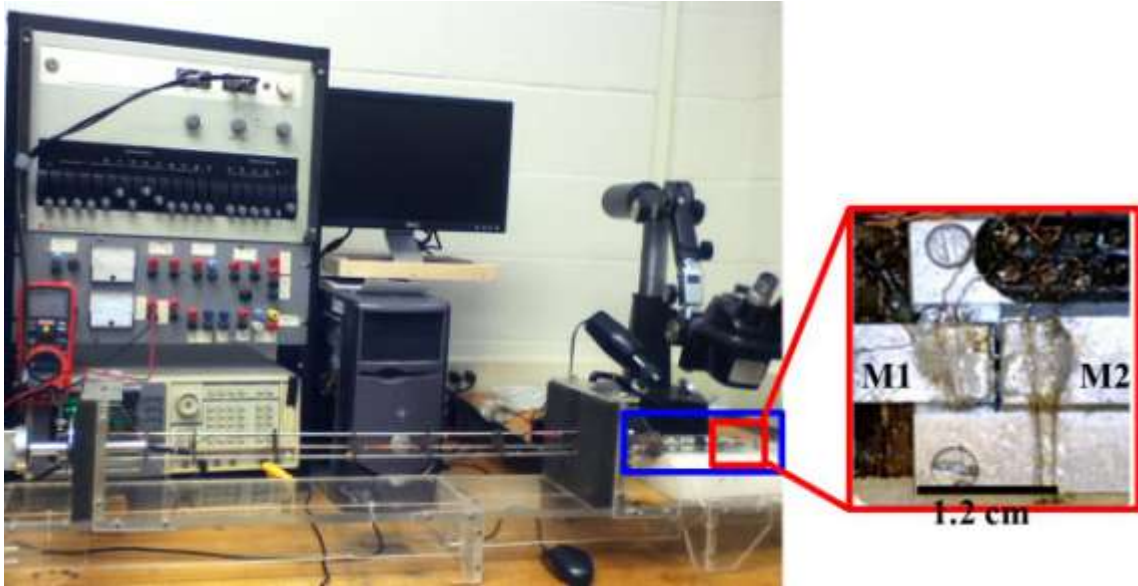


Figure 10. Picture of the fiber puller on a bench top table. The stress-strain device of the fiber puller is located in the blue square and mounting plates M1 and M2 are shown in a zoomed view inside red squares.

### 3.3 Equipment Calibration

Following the puller device diagram in Figure 9 and its operation in the above section, we see that the force  $F$  applied to the sample is a function of the current  $I$  which creates a magnetic field that acts on the built-in permanent magnets, so:

$$F = c_F * I \quad (18)$$

where:  $c_F$  is the force constant in N/A. The force-current relation was calibrated by a hanging weight attached to a micromanipulator to the movable plate (M1), moving the weight with the micromanipulator and returning M1 to its equilibrium position by adjusting the current in the coil. A schematic diagram of the force balance is shown in Figure 11. The force on the pulling magnet  $F_p$  was linear in current with a slope of  $\Delta F_p/\Delta I = 0.562 \pm 0.01$  N/A. A plot of  $F$  vs.  $I$  is shown in Figure 12. Similarly, a force constant was also determined for the oscillating magnet which applies an oscillating force to monitor relative changes in Young's modulus. A slope of  $\Delta F_o/\Delta I = 0.176$  N/A was obtained resulting in a  $F_p:F_o$  ratio of 3.2.

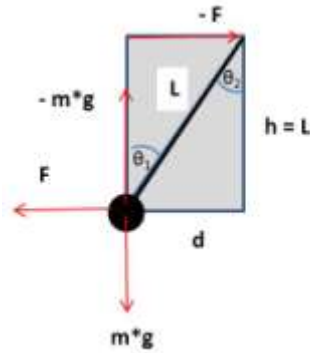


Figure 11. Schematic diagram of the force balance in the force-current calibration.

The fiber puller uses a capacitive technique to correlate the change in capacitance with the elongation of the sample. The SRS 850 lock-in amplifier measures the off-balance of the capacitance bridge. The capacitance is proportional to the offset according to the relation:

$$C = C_0 - (c_C * X) \quad (19)$$

where:  $C$  is the final capacitance (pF),  $C_0$  is the initial capacitance (pF),  $X$  is the offset in mV and  $c_C$  is the capacitance constant in pF/mV. The final capacitance was linear in offset with a slope of  $\Delta C/\Delta X = 1.42 \pm 0.006$  pF/mV. A plot of  $C$  vs.  $X$  is shown in Figure 13.

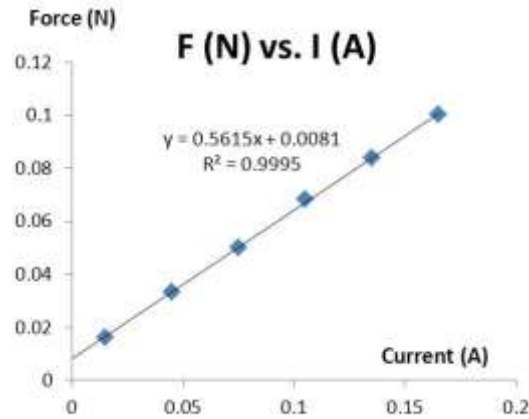


Figure 12.  $F$  vs.  $I$  calibration plot showing a slope of 0.5615 N/A.

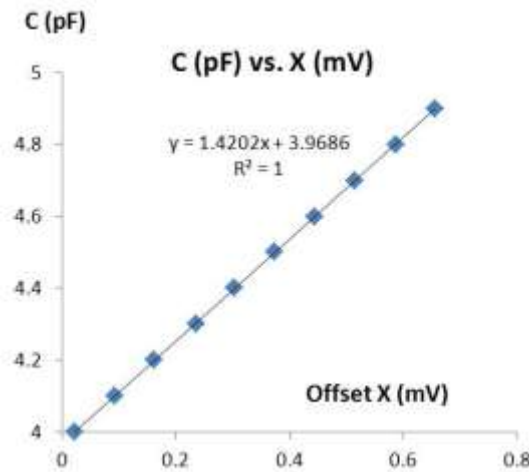


Figure 13.  $C$  vs.  $X$  calibration plot showing a slope of 1.42 pF/mV.

The change in capacitance  $\Delta C$  is inversely proportional to the change in length of the sample  $\Delta L$  in  $\mu\text{m}$ , *i. e.*, the displacement  $\Delta d$  of the capacitor plate CP1 according to the relation:

$$\Delta d = c_d * \left( \frac{1}{C_0} - \frac{1}{C} \right) \quad (20)$$

where:  $c_d$  is the displacement constant in  $\mu\text{m.pF}$ . The  $\Delta d-1/C$  relation was calibrated by measuring the displacement of a specific spot on M1 with the change in current using an optical microscope with a calibrated reticule. The capacitance change was also measured simultaneously. Figure 14 depicts a linear relationship between displacement and  $1/C$  over a wide range. The displacement constant  $c_d$  was calculated to be  $2061.9 \pm 86.2 \mu\text{m.pF}$ .

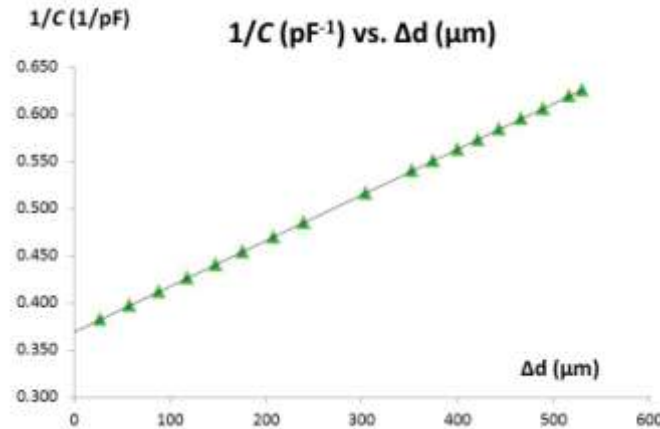


Figure 14.  $1/C$  vs.  $\Delta d$  calibration plot.

The tensile stress and strain applied to the sample are calculated using equations (1) and (2). The calculated force given by equation (18) is the total force  $F_T$  and not the

force  $F_{sam}$  acting on the sample and, therefore, this force must be calculated. Taking into consideration the spring constant of the leaf spring supports for the center rod of the apparatus ( $k = 0.065 \text{ mN}/\mu\text{m}$ ) the force on the sample is given by<sup>45</sup>:

$$F_{sam} = F_T - k \Delta d \quad (21)$$

Once all variables are calculated the stress and strain can be obtained as well as the second-order elastic constant (or Young's modulus) according to equation (5).

### **3.4 Equipment Automation**

During and after calibration of the fiber puller all measurements were taken by hand meaning that the equipment was lacking some form of computer control. It was also part of this project to design a program capable of collecting data of the tensile measurements so equipment and experiment control were possible for further data analysis. LabVIEW<sup>®</sup> from National Instruments is the program used to automate the fiber puller. The program, initially, recorded the basic variables: lock-in amplifier offset (related to strain) and current (related to force) only. All other variables were calculated in a spreadsheet using the calibration relationships after calibration constants were determined. At that early stage of program development manual and automated data were put side by side to make sure the program was delivering comparable results. Once reliability was achieved manual data collection was eliminated.

It is to be mentioned that the process of program development did not take place at once. Continuous development of the program took place throughout the past two

years, and there is still room for improvement. For the purposes of the project the present program has served well its function. An overview of the LabVIEW<sup>®</sup> program used to control the fiber puller is introduced next.

A snapshot of the front panel of the main LabVIEW<sup>®</sup> program is shown in Figure 15. In the “Sample Properties” box, besides the file name, characteristics of the sample, such as: gauge length, fiber diameter, initial capacitance and cross-sectional area of the fiber are entered. Fiber diameter and cross-sectional area were fixed for these experiments, but file name, gauge length and initial capacitance differ for each experiment and sample.

In the “System Controls” box, parameters that can control the experiment are entered. “Current max” limits the total force applied to the sample; “current step” controls the current (or force) increment applied to the sample from start to end, “time for output to stabilize” controls the duration each measurement is held until the next measurement is taken and, “time to wait” tells the instrument how long it should hold the last measurement taken (at the maximum force) before the puller starts to release (or unload) the fiber. It is worth mentioning that the program is designed to pull the fiber to a specific maximum force and unload it back to zero force so hysteresis curves can be obtained.

The “Oscillation Controls” box controls the second lock-in amplifier (EG&G 5110) which applies oscillation forces to the coil magnet and oscillates the sample. “Oscillation current” can be set on or off, “oscillation time” controls the duration the coil oscillates in each measurement and, “oscillation amplitude” controls the amplitude of

oscillation. The frequency of oscillation is set manually in the EG&G 5110 lock-in amplifier before the experiment is started.

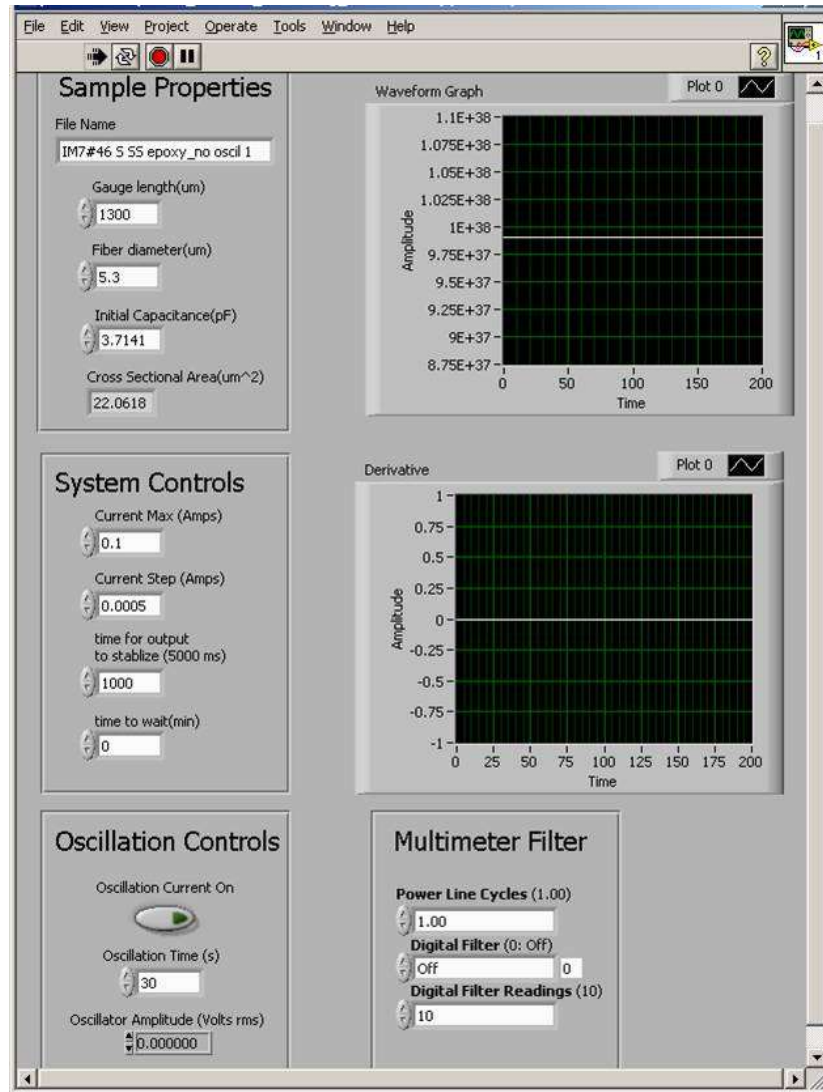


Figure 15. Snapshot of the front panel of the main LabVIEW<sup>®</sup> program used to control the tensile measurements on the fiber puller.

“Waveform Graph” in the front panel plots the amplitude of the output of the first lock-in in volts *versus* data points for the pulling data. The “Derivative” graph plots the

amplitude of the output of the second lock-in in volts *versus* data points for the pulling data.

The “Multimeter Filter” box controls the parameters of the filter; “power line cycles” determines the type of averaging, “digital filter” on or off and “digital filter readings” set the number of points being averaged.

The data from each run is saved in a file that can be opened in Excel. The spreadsheet records the following information: trace X (V), total force (mN), capacitance (pF), distance ( $\mu\text{m}$ ), strain, force on sample (mN), stress (GPa), second lock-in output (V) and oscillating distance ( $\mu\text{m}$ ). The stress *vs.* strain curve is plotted using Excel tools and HOECs are obtained by fitting the strain-stress plot with a three term polynomial regression. Results and discussion are presented in the next chapter.

## CHAPTER FOUR

### RESULTS AND DISCUSSION

#### 4.1 Surface Morphology Characterization

Sample characterization using a field emission scanning electron microscope (SEM), model Hitachi S4800 showed an average filament diameter of  $5.3 \pm 0.2 \mu\text{m}$  obtained from 27 dissimilar IM7 pieces, which is in good agreement with the diameter of 5.2 microns reported by the manufacturer. Figure 16 shows the surface morphology of a single filament of the IM7 carbon fiber obtained by SEM analysis.

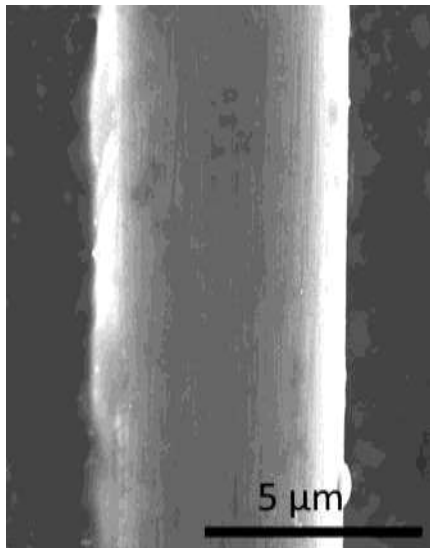


Figure 16. SEM image of a single filament of IM7 carbon fiber with diameter of 5.3 microns.

## 4.2 Elastic Properties

The tensile modulus was determined by plotting a stress *versus* strain curve and fitting it with linear and polynomial regression. The average Young's modulus obtained for 42 runs was  $242.8 \pm 21.6$  GPa by linear regression and  $230.8 \pm 20.2$  GPa by polynomial regression. The reason for these differences will be discussed later. Fibers of gauge length between 2.2 and 5.5 mm were tested. The Young's modulus reported by the manufacturer is 276 GPa, which was determined by test method ASTM D3039 designated as "Standard Test Method for Tensile Properties of Polymer Matrix Composite Materials". A study published in 2010 by Qian *et al.*<sup>46</sup> reported a Young's modulus value of 298 – 299 GPa for single filaments of IM7 carbon fiber with gauge lengths ranging from 15 to 35 mm. Their tests were carried out on a single filament using a tensile testing rig instrument following the standard method BS ISO 11566:1996 designated as "Standard Test for Determination of the Tensile Properties of Single Filament of Carbon Fiber Specimens". We would expect their  $E$  to be larger than the manufacturer's because they did not allow for a finite higher-order elastic behavior. Since the fiber puller used in the studies for this Thesis was designed and built to accommodate custom made samples of micro-scale size, no standard method was followed.

The ultimate fiber elongation at failure (maximum strain %) is reported by the manufacturer as 1.9 % for the HexTow<sup>®</sup> IM7-12K. Using the average Young's modulus

---

<sup>46</sup> H. Qian, A. Bismarck, E. S. Greenhalgh, M. S. P. Shaffer, *Carbon Nanotube Grafted Carbon Fibres: A Study of Wetting and Fibre Fragmentation*, Composites: Part A **41**, 1107-1114, 2010.

obtained above and considering the maximum strain (nearly 2.2 %) applied to the samples, a lower limit range for the tensile strength of a single filament of IM7 can be estimated between 4.21 and 5.02 GPa (compared to 4.84 – 5.89 GPa for a single filament by Qian *et al.*<sup>46</sup> and 5.67 GPa for the tow reported by the manufacturer). However, the majority of the single filaments tested did not break at the maximum forces applied which were around 101.2 mN. The higher breaking strains may be due to the shorter length of the samples which may imply probabilities of fewer defects within and on the graphitic structure<sup>47</sup> of the shorter carbon fiber filaments. The fact that these tests were performed on single filaments instead of the entire tow is also considered. Single filament tests result in a higher modulus since the single fiber is correctly aligned, while in a tow not all filaments are parallel, resulting in a lower modulus<sup>9</sup>.

Figure 17 shows the hysteresis loops of five runs of a single filament of the IM7 carbon fiber glued with Devcon<sup>®</sup> S-31, 2 ton clear weld epoxy. The respective sample bow profile (which is related to how much the fiber is straightened before pulling begins) for each run is also shown. The more straightened the fiber before pulling begins (run 5 in Fig. 17), the closer to the origin the stress-strain curve will begin, *i. e.*, the stress-strain curve will start at zero. Although the loops are narrow, one can see the relatively good definition of the hysteresis loops. According to Wang *et al.*<sup>48</sup> this behavior indicates that very little damage occurred within the fiber during the tensile load/unload cycle. It is clear that a small residual strain is left behind after the sample is unloaded. There are two

---

<sup>47</sup> M. S. Dresselhaus, G. Dresselhaus, K. Sugihara, I. L. Spain, H. A. Goldberg, *Graphite Fibers and Filaments*, Springer Series in Materials Science **5**, Springer-Verlag, 1988.

<sup>48</sup> Y. Wang, L. Zhang, L. Cheng, H. Mei, J. Ma, *Characterization of Tensile Behavior of a Two-Dimensional Woven Carbon/Silicon Carbide Composite Fabricated by Chemical Vapor Infiltration*, Materials Science and Engineering: A **497**, 295-300, 2008.

reasons for this behavior: a) the energy stored by the fiber during pulling is not completely released during unloading and leaves behind a residual strain, or b) there was a slight slipping of the sample through the glue.

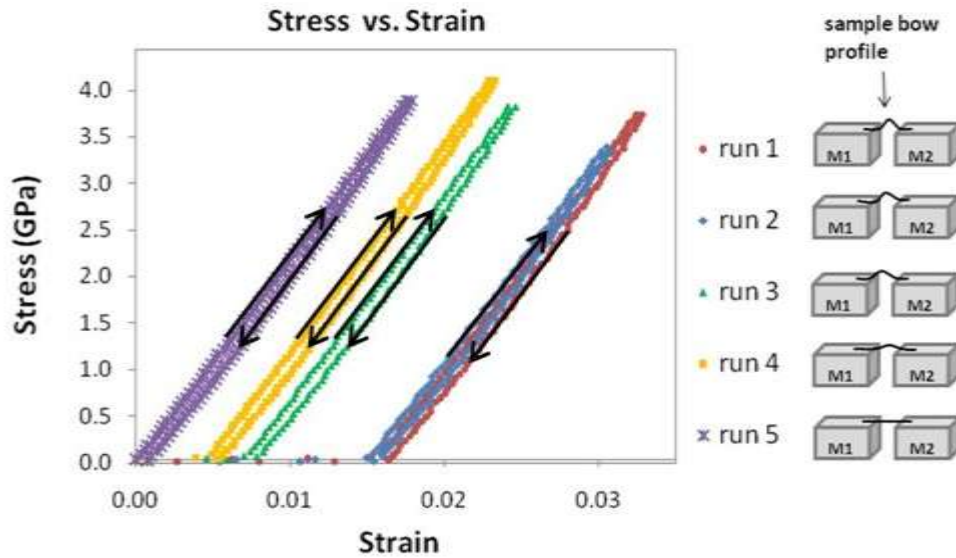


Figure 17. Hysteresis loop of five runs of a single filament of the IM7 carbon fiber with the respective sample bow profile for each run. M1 and M2 represent the movable and stationary sample mounting plates, respectively (refer to Fig. 9). The arrows up represent the loading (pulling) of the sample and the arrows down represent the unloading (releasing).

Figure 18 shows an example of linear and polynomial regression fits in the stress vs. strain plot for the single filament sample ID IM7 #42, run 3, glued with Devcon<sup>®</sup> S-6, plastic steel weld epoxy. The linear fit is represented by a continuous red line and the polynomial fit is shown in a dashed black line. From the fitting equations shown in the figure one can see that the polynomial fit is a much better fit to the data obtained. It can

be noted that the stress-strain curve is steep and straight without noticeable softening. According to Lee *et al.*<sup>49</sup> this is an indication of negligible plastic deformation in the sample. The positive constant value multiplying the  $x^2$  term in the polynomial fit equation (+992.66 GPa) is also an indication of very little, or non-existent fiber slippage during pulling. The fiber was pulled to a total strain of 1.03 % at an applied stress of 2.42 GPa at a maximum force of 56.2 mN. For this particular run, the value obtained for the Young's modulus was 235.37 GPa by linear regression and 225 GPa by polynomial regression. A fit to the data which includes higher-order terms results in a lower estimate of Young's modulus,  $E$ . The green curve represents the nonlinear portion of the polynomial fit and it shows us that there is, indeed, a nonlinear behavior of this fiber that is unnoticeable to the eye in the linear regression. This proves the existence of HOECs (third-order, fourth-order, etc.). The HOECs are a consequence of the interatomic forces not being strictly parabolic.

The HOEC was determined by plotting a strain vs. stress curve and fitting it to polynomial regression. To calculate the value of the inelastic constant,  $\delta$  was factored by  $s_{11}$ , according to equation (16). The average value obtained for  $\delta$  was  $-2.9 \pm 1.7$  which represents a combination of the individual elastic coefficients. This value was more consistent and reproducible for fibers of longer gauge length (between 2.2 and 5.5 mm) than for fibers of relatively shorter gauge length (between 1 and 1.5 mm). The average value of the elastic constant  $s_{11}$ , which is inversely proportional to Young's modulus, was

---

<sup>49</sup> C. Lee, X. Wei, Q. Li, R. Carpick, J. W. Kysar, J. Hone, *Elastic and Frictional Properties of Graphene*, *Physica Status Solidi B* **246**, 2562-2567, 2009.

calculated to be  $4.2 \pm 0.35 \times 10^{-3} \text{ GPa}^{-1}$  by linear regression. By polynomial regression  $s_{11}$  was found to be  $4.4 \pm 0.37 \times 10^{-3} \text{ GPa}^{-1}$ .

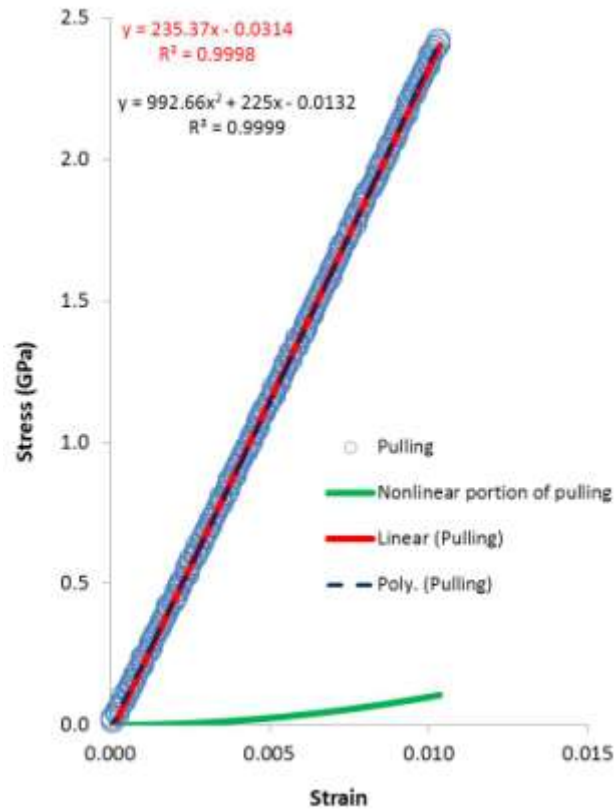


Figure 18. Stress vs. strain pulling plot of an IM7 fiber. The linear fit is represented by a continuous red line and the polynomial fit is shown in a dashed black line. The green curvature represents the nonlinear portion of the pulling data which is represented by open blue circles.

Figure 19 shows the strain vs. stress curve (open blue circles) for the sample ID IM7 #42, run 3 (which it is just the inverse plot from Figure 18). The linear fit is represented by a continuous red line and the polynomial fit is shown in a dashed black

line. The polynomial fit is shown to be a better fit to the data according to the fitting equations. The nonlinear portion of the polynomial fit is represented by a green line and its downward curvature originates the negative sign of the nonlinearity constant,  $\delta$ .

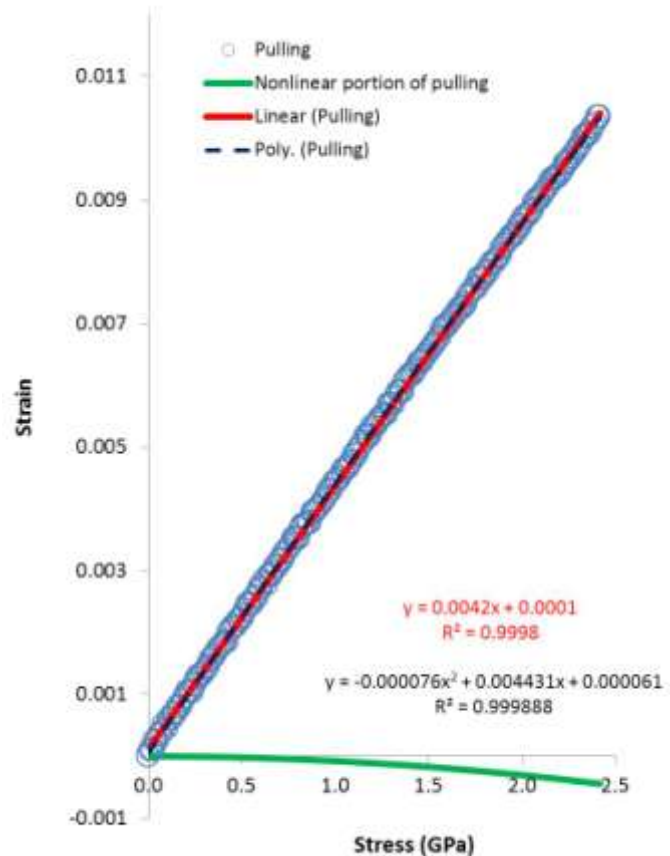


Figure 19. Strain vs. stress plot (open blue circles) for an IM7 sample (inverse to the plot in Figure 18). The polynomial fit is represented by a dashed black line. The green curvature represents the nonlinearity in the strain-stress relation.

In order to verify the nonlinearity of the slope of the stress-strain relation, a second lock-in amplifier (EG&G 5110 in Fig. 9) was coupled to the fiber puller system.

Here, a small oscillating force is applied by an oscillating current in a separate coil around the magnets that apply force to the center rod and thus to the sample. This oscillating force provokes an oscillating strain in the sample, and thus an oscillating capacitance that is measured by the bridge off-balance and the SRS 850 lock-in amplifier that measures this off-balance. The second lock-in (tuned to a much lower frequency than the one used in the capacitance bridge) takes the output of the first lock-in and measures the component of the signal at the oscillating frequency, 5.12 Hz. This signal is inversely proportional to the slope of the stress strain curve. The data is given in terms of the inverse voltage *versus* strain %. Figure 20 shows an example of this data collected for an IM7 sample of gauge length 4.0 mm. The stress *vs.* strain curve for this particular sample is consistent with previous data showing the curve to be steep and straight with very little noticeable curvature. A constant voltage of 1.5 V and frequency of 5.12 Hz were applied to the oscillating magnet coil. The delay time between each measurement was 8 s. The maximum force applied by the pulling coil was 56.2 mN with increments of 0.3 mN and delay times of 1.5 s between each measurement. This corresponded to a total strain of 0.75 % and maximum applied stress of 2.10 GPa. No damage (breaking) of the sample was observed in this case. The secondary y-axis in Figure 20 corresponds to the inverse of the output voltage of the second lock-in *versus* the strain. Interestingly, one can note the curvature (polynomial regression fit of the  $1/V$  *vs.* strain % plot) of the slope in the strain region at which the sample is being straightened confirming that the curvature is related to the HOECs (third- and fourth-order) pertained to this type of fiber.

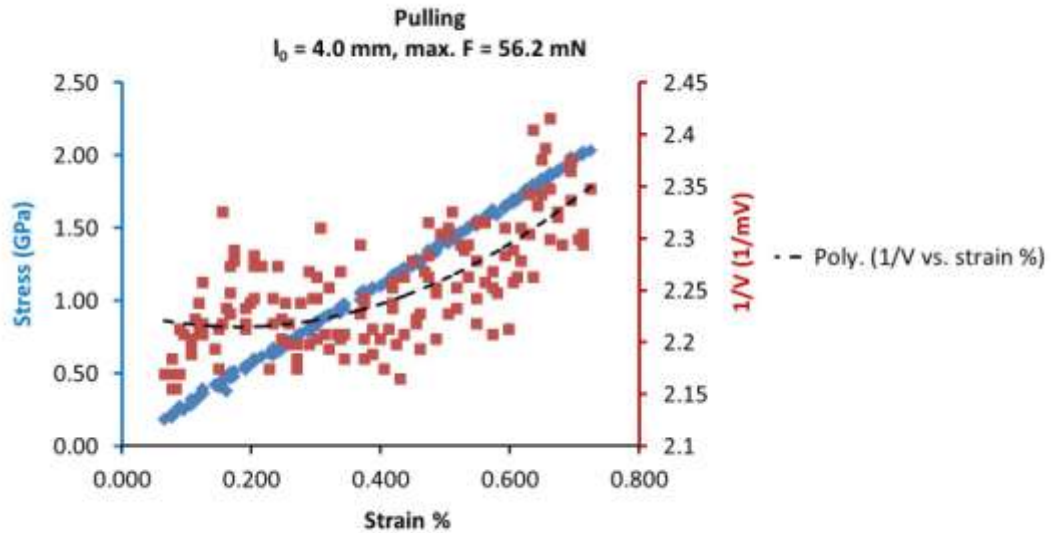


Figure 20. Stress vs. strain % pulling plot of an IM7 sample of gauge length 4.0 mm (diamond shaped blue points) and  $1/V$  vs. strain % correspondent to it (square shaped red points). The dashed lines represent a polynomial fit to the  $1/V$  vs. strain % plot and it is a guide to the eye. The curvature of the slope of the stress-strain relation is highly accentuated by the use of a second lock-in amplifier.

As previously mentioned, the oscillating amplitude of the output voltage is inversely proportional to the slope of the stress-strain plot. An example of this proportionality can be seen in Figure 21. The primary y-axis shows the normalized  $d\sigma/d\varepsilon$  vs. strain (blue line) and the secondary y-axis shows the normalized  $1/V$  vs. strain (red trace) corresponding to it. The dashed black line is a linear fit to the normalized  $1/V$  vs. strain and one can see that its change is around 6%. Comparatively, the change observed for the normalized  $d\sigma/d\varepsilon$  vs. strain is around 6% as well. The second lock-in gave results

that agree with the analysis of the first; that is, the slope of the stress-strain curve increases gradually and at a constant rate. This agreement between the two ways of measuring the nonlinearity gives more confidence in its measurement.

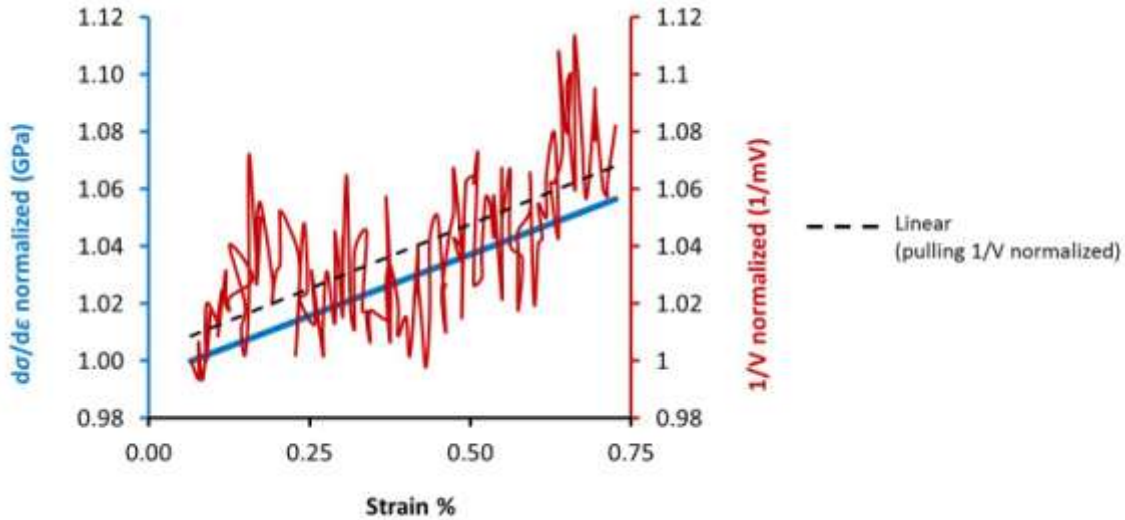


Figure 21. Normalized plots of the  $d\sigma/d\varepsilon$  vs. strain % (blue line) and  $1/V$  vs. strain % (red trace). The dashed black line is the linear fit of the normalized  $1/V$  vs. strain plot, and is a guide to the eye. Both slopes are in good agreement with each other, being approximately 6% change each.

The observation of nonlinear elasticity in carbon fibers is explained by a strain-induced stiffening mechanism<sup>14</sup> which generates an initial and final modulus associated with the increased strain imposed on the sample. Table 1 shows the values of Young's modulus obtained by both linear and polynomial regression fits for an IM7 sample of gauge length 3.1 mm. We note that the higher the strain the higher is the value of the tensile modulus. Small strains (0.6 %) at the initial stage give rise to lower slopes (249

GPa) while at larger strains (1.7 %) a final slope with a higher value is obtained (262 GPa). A fit to the data which includes higher-order terms results in a lower estimate of Young's modulus,  $E$ . This may be the reason that our values of  $E$  are lower than published values, and the reason that  $E$  as measured by the best linear fit is larger when a larger strain is applied to the sample. If the isothermal  $E$  is defined as the second derivative of the Gibbs energy with respect to stress, evaluated at zero stress, then it is determined by the linear term in a polynomial fit to a stress-strain curve.

Table 1. Values of Young's modulus obtained by both linear and polynomial regression fits for an IM7 sample of gauge length 3.1 mm. The maximum strain % applied for each run is also listed. Note that  $E$  as measured by a linear fit increases monotonically with strain, whereas  $E$  as measured by a polynomial fit is relatively constant.

<b>Run #</b>	<b>Max. strain %</b>	<b><math>E</math> (GPa), linear fit</b>	<b><math>E</math> (GPa), polynomial fit</b>
1	0.6	249	238
2	1.2	252	235
3	1.7	262	244

In 1969 Ruland<sup>50</sup> elucidated the reason for the increase of the carbon fiber's modulus developing an elastic unwrinkling model. He assumed that the graphitic layers of a carbon fiber are connected together to form long and wrinkled ribbons along the

---

<sup>50</sup> W. Ruland, *The Relationship Between Preferred Orientation and Young's Modulus of Carbon Fibers*, Applied Polymer Symposia **9**, 293-301, 1969.

fiber axis. When the fiber is subjected to tensile forces, a stress on the ribbons increases the preferred orientation of the individual layers; consequently, the stiff axis of the individual layers is more directly aligned with the fiber axis resulting in an increased fiber modulus.

### 4.3 Electrical Properties

Figure 22 shows the change in resistance with increasing strain during pulling for an IM7 sample of gauge length 4.3 mm. The measurements were taken over a force ranging from zero to 84.3 mN with increments of 0.6 mN. The delay times between each measurement were 0.1 (runs 15-18), 1 (runs 6-10) and 5 (runs 11-14) seconds.

From the figure, one can see the increase in resistance with increasing strain for all 13 runs. The average value obtained for the variation of the scaled resistance with strain,  $(1/R) dR/d\varepsilon = (1/\rho) d\rho/d\varepsilon$ , was  $1.27 \pm 0.10$  ( $\Omega\cdot\text{cm}/\Omega\cdot\text{cm}$ ) which is in good agreement with Blazewicz et al.<sup>51</sup> who studied the piezoresistance effect in different types of carbon fibers. The average value of the resistivity of the fiber was calculated to be  $1.52 \pm 0.12 \times 10^{-3}$   $\Omega\cdot\text{cm}$ , which is in good agreement with the electrical resistivity of the tow ( $1.5 \times 10^{-3}$   $\Omega\cdot\text{cm}$ ) reported by the manufacturer. These results are also in agreement with Owston<sup>52</sup> who measured the electrical resistance of single PAN-based carbon fibers with 8  $\mu\text{m}$  diameters and gauge lengths from 45 to 250 mm using a

---

<sup>51</sup> S. Blazewicz, B. Patalita, P. Touzain, *Study of Piezoresistance Effect in Carbon Fibers*, Carbon **35**, 1613-1618, 1997.

<sup>52</sup> C. N. Owston, *Electrical Properties of Single Carbon Fibres*, Journal of Physics D **3**, 1615-1626, 1970.

tensometer. The authors attributed these results to be between 10 and 100 times the values of the resistivity for the basal plane conduction in graphite single crystals, which is about  $4 \times 10^{-5} \Omega \cdot \text{cm}$  at room temperature<sup>53</sup>. The origin of the electrical noise may come from a somewhat granular structure of the fibers with contacts between the grains which may tend to rupture under higher tensile loads<sup>52</sup>.

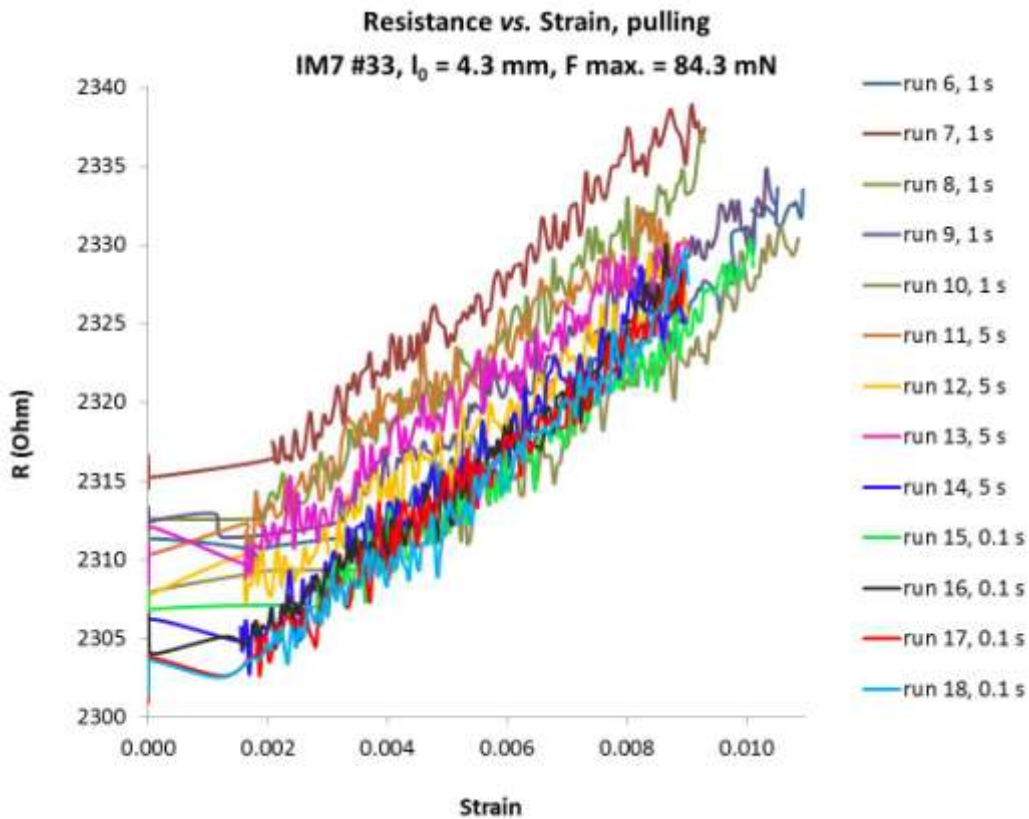


Figure 22. Resistance vs. strain plot of an IM7 sample. The times, 0.1, 1 and 5 s correspond to the duration of the force applied between each measurement.

<sup>53</sup> D. W. McKee, *Carbon and Graphite Science*, Annu. Rev. Mater. Sci. **3**, 195-231, 1973.

Figure 23 shows the hysteresis loop for  $R$  vs.  $\epsilon$  for run 15 in Figure 22. The blue line is loading (pulling) and the red line, unloading (releasing). The hysteresis loop profiles of the resistance measurements were very similar to those obtained during tensile tests (narrow and well defined for all runs).

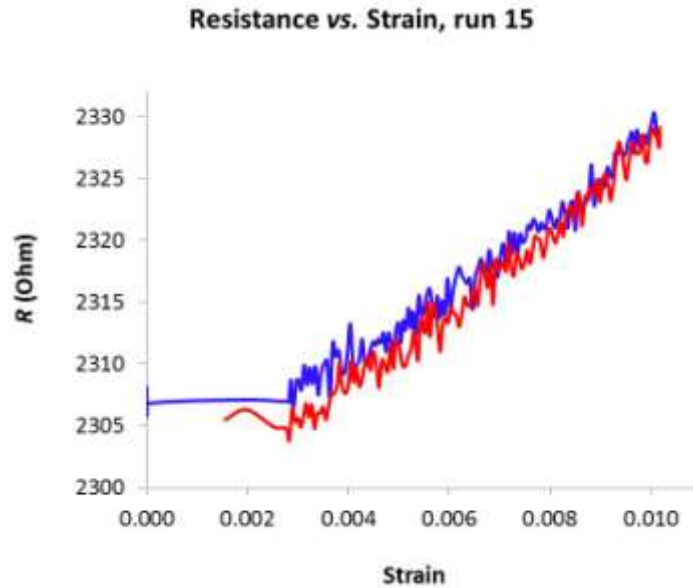


Figure 23. Hysteresis loop for the resistance vs. strain for the run 15 in Figure 22. The blue line is loading (pulling) and the red line, unloading (releasing).

It can be seen that the final resistance after complete unload did not return to its original value which is typical carbon fiber behavior under high loading conditions<sup>52</sup>. The piezoresistivity mechanism in carbon fibers has been explained by different authors in terms of the change in electrical resistance with strain, being due to changes in the

contact resistance between the grain boundaries of the fiber<sup>54</sup>, or the degree of misorientation between the crystallites in the fiber<sup>55</sup>, or the density of dangling bonds in the atomic hexagonal graphite structure of the carbon fiber<sup>56</sup>.

#### **4.4 Contribution of epoxy (glue) to the Young's Modulus of Carbon Fiber**

In order to maintain a sample secured on the fiber puller mounting plates during tensile measurements the sample must be glued at both ends with glue (or epoxy). The first tensile experiments performed on IM7, with either manual or automated collection of data, used Devcon<sup>®</sup> S-205 high-strength 5-minute epoxy. At that early stage of equipment calibration and automation, the results for second- as well as third-order elastic constants were low and inconsistent. The S-205 5-min epoxy served its purpose but it seemed, according to the results, that the fiber was slipping through it, producing unreliable data. In order to obtain improved results, a search for a better epoxy was undertaken.

Several different types of glue were tried, and all failed to secure the fiber adequately during tensile measurements except epoxy glue. The glues tried were: super glue, sodium silicate and diphenylcarbazide. A combination with different two types was also tried unsuccessfully. Then Devcon<sup>®</sup> S-31, 2 ton clear weld epoxy was tried, and the

---

<sup>54</sup> M. Endo, Y. A. Kim, T. Hayashi, K. Nishimura, T. Matusita, K. Miyashita, M. S. Dresselhaus, *Vapor-Grown Carbon Fibers (VGCFs): Basic Properties and their Battery Applications*, Carbon **39**, 1287-1297, 2001.

<sup>55</sup> P. C. Conner, C. N. Owston, *Electrical Resistance of Single Carbon Fibres*, Nature **223**, 1146-1147, 1969.

<sup>56</sup> Y. Nishi, T. Toriyama, K. Oguri, A. Tonegawa, K. Takayama, *High Fracture Resistance of Carbon Fiber Treated by Electron Beam Irradiation*, J. Materials Research **16**, 1632-1635, 2001.

results obtained were more consistent and reproducible than the results obtained with 5-min epoxy. New experiments were performed for acquisition of new data and all previously obtained data were discarded.

Although the data obtained with Devcon<sup>®</sup> S-31 epoxy seemed to be in good agreement with the manufacturer, it was the oscillation experiments that raised doubts about this glue and how well it was working to keeping the carbon fiber in place without slippage. A helpful clue to determine if the fiber is slipping through the glue during tensile measurements is to pay attention to the quadratic term in a polynomial fit to the stress-strain curve. If that term is negative, there is an indication of fiber slippage. The resulting data from oscillation experiments does not account for fiber slippage, because the time constant associated with slippage appears to be much longer than that associated with the oscillation frequency. Therefore, oscillation measurement is a second way of confirming the presence of HOECs of a sample, but is limited in its usefulness in measuring glue slippage. From experience and analyzing the hysteresis response and the final strain after unloading, one might notice a broadening of the hysteresis behavior, which suggests that some slippage of the fiber in the glue might be occurring.

In order to answer this question another type of epoxy was tried, Devcon<sup>®</sup> S-6 high-strength plastic steel epoxy. This epoxy gave the best results for IM7 elastic properties, “best” meaning the highest values for modulus obtained thus far. Another observation throughout the course of the project was that shorter fibers had lower modulus than longer ones. Understanding that the glue was playing a role in the resulting

measured value for the HOECs, a model was proposed to correlate the values of the measured modulus with the actual one.

Assuming that a carbon fiber sample of initial length  $l_1$ , and homogeneous diameter throughout its length, subjected to a force  $F$  will deform  $\Delta l_1$ , and assume that the deformation in the glue will be  $\Delta l_g$ . Cutting the fiber to a shorter length  $l_2$ , regluing it and subjecting it to the same force  $F$ , the fiber will deform  $\Delta l_2$ . Assuming that the deformation in the glue is the same for both lengths, we have:

$$\Delta l_1 = \frac{l_1 \cdot F}{A_1 \cdot E} + \Delta l_g \quad (22)$$

$$\Delta l_2 = \frac{l_2 \cdot F}{A_2 \cdot E} + \Delta l_g \quad (23)$$

$$\Delta l_g = c \cdot F \quad (24)$$

It is known that the Young's modulus is the ratio between stress and strain, and strain is  $\Delta l/l$ . Using the relations in equations (22), (23) and (24) we obtain for the measured modulus  $E_{m1}$  and  $E_{m2}$ :

$$E_{m1} = \frac{F / A_1}{\varepsilon_1} = \frac{F / A_1}{F / A_1 E + cF / l_1} \quad (25)$$

$$E_{m2} = \frac{F / A_2}{\varepsilon_2} = \frac{F / A_2}{F / A_2 E + cF / l_2} \quad (26)$$

Rearranging equations (25) and (26) we obtain:

$$E_{m1} = \frac{E}{1 + k / l_1} \quad (27)$$

$$E_{m2} = \frac{E}{1 + k / l_2} \quad (28)$$

$$k = c.A.E \quad (29)$$

Solving equation (27) for  $k$  and putting it into equation (28) we have:

$$k = l_1 \left( \frac{E}{E_{m1}} - 1 \right) \quad (30)$$

$$E_{m2} = \frac{E}{1 + \frac{l_1}{l_2} \left( \frac{E}{E_{m1}} - \frac{l_1}{l_2} \right)} \quad (31)$$

Solving for the actual modulus  $E$  we have:

$$E = \frac{l_1 - l_2}{\frac{l_1}{E_{m1}} - \frac{l_2}{E_{m2}}} \quad (32)$$

Applying equation (32) to the resulting measured modulus of a non-oscillating IM7 sample (ID IM7 #42) glued with Devcon<sup>®</sup> S-6 high-strength plastic steel epoxy of longer length 3.9 mm and shorter length 2.2 mm, the actual tensile modulus obtained was 307 GPa. This result confirms the tensile modulus of a single filament to be higher than the modulus reported for a fiber tow due to a better alignment of the single fiber compared to multiple fibers within a bundle. The actual modulus is higher than the upper and lower values of measured modulus fitted to polynomial regression ( $258.1 \pm 5.6$  and  $229.7 \pm 6.1$  GPa, respectively). An average of six runs for the 3.9 mm fiber was used while 5 runs were used for the 2.2 mm IM7 piece. For these runs the maximum applied force ranged from 45 to 101.2 mN and the total strain varied from 0.7 to 1.9 %. None of these fibers failed (broke). Once again, to confirm the contribution of the glue to the measured modulus of the single carbon filament, the same correction was applied to the measured moduli of two pieces of the same tungsten wire of lengths 4.2 mm and 2.2 mm.

The results were consistent with the correction for the IM7, that is the accepted value of  $E$  was obtained only by correcting for the contribution of the glue to the measured strain. This is further evidence that the epoxy used to secure the sample on the fiber puller has an effect on the final measured tensile modulus of samples.

## CHAPTER FIVE

### CONCLUSIONS

Young's modulus, the resistivity, the piezoresistivity and  $\delta$ , the nonlinearity in the stress-strain relation for single filaments of IM7 carbon fibers have been successfully measured. It is shown that  $\delta$  is related to a combination of second- and third-order elastic constants. Since these are derivatives of the Gibbs free energy with respect to stress or strain, they are relatively easy to compare to calculations from a model of the structure of the fibers.

Results from this work also showed strain-induced stiffening effects pertain to carbon fibers. The higher the strain applied to the sample, the higher the tensile modulus obtained. Likewise, a comparison between the Young's modulus obtained by linear regression and polynomial regression revealed that a linear fit gives higher values. The presence of higher-order elastic terms, which are neglected in a linear fit, causes a decrease in the reported value of the second-order elastic constant, but a value consistent with thermodynamic definitions of the elastic moduli.

The use of a second lock-in amplifier, coupled to the fiber puller system, confirmed the presence of HOECs since the results were proportional to the derivative of the stress-strain relation.

Moreover, a correction for the contribution of the epoxy to the measured tensile modulus of single filaments of IM7 carbon fiber was applied, and it was revealed that the epoxy plays a role during tensile measurements. The actual calculated tensile modulus of single filaments of IM7 is higher than the measured values, reaching 307 GPa, compared

to 276 GPa modulus for the fiber tow reported by the manufacturer. It is expected that these results may be of interest for theoretical modeling and simulations, and help researchers in attaining a better understanding of the properties and behavior of composites which incorporate IM7 carbon fiber.

## CHAPTER SIX

### RECOMMENDATIONS FOR FUTURE WORK

The fiber puller has been successfully applied to the determination of the elastic properties of IM7 carbon fiber. A second lock-in amplifier coupled to the instrument helped in confirming the presence of HOECs in this sample. It is recommended that any type of carbon fiber, or any type of micro-scale size sample be tested using the equipment. Materials that do not have their  $E$  determined can be subjected to tensile measurements and their elastic properties can be measured, aiding in helping scientists who specialize in modeling and simulations. Additionally, the LabVIEW<sup>®</sup> program is open to improvement. Any further relation or calculation can be added to the program. It is the intent to develop the current program further and code it to perform consecutive, or continuous, loading and unloading cycles for study of hysteresis behavior with increasing strain sequences. The use of epoxy to hold samples in place should be taken into consideration and each different type of glue should be investigated to determine their individual contribution to the measured tensile modulus of samples.